# Structural basis for mTORC1 regulation by the CASTOR1-GATOR2 complex

**Rachel Jansen**
UC Berkeley
**Clement Maghe**
University of California, Berkeley
**Karla Tapia**
University of California, Berkeley
**Selina Wu**
University of California, Berkeley
**Serim Yang**
University of California, Berkeley
**Xuefeng Ren**
University of California, Berkeley https://orcid.org/0000-0002-4822-4316
**Roberto Zoncu**
University of California, Berkeley https://orcid.org/0000-0003-1611-1891
**James Hurley**
jimhurley@berkeley.edu

University of California, Berkeley https://orcid.org/0000-0001-5054-5445

**Biological Sciences - Article**

**Keywords:**

**Posted Date:** May 13th, 2025

**DOI:** https://doi.org/10.21203/rs.3.rs-5073364/v1



**Additional Declarations: Yes** there is potential Competing Interest. J.H.H. is a co-founder and shareholder of Casma Therapeutics, has received research funding from Genentech and Hoffmann-La Roche, and has consulted for Corsalex. R.Z. is a cofounder and shareholder of Frontier Medicines,

science advisory board member for Nine Square Therapeutics and receives research funding from Genentech. The other authors declare no competing interests.

**Title:** Structural basis for mTORC1 regulation by the CASTOR1-GATOR2 complex

**Authors:** Rachel M. Jansen[1,2], Clément Maghe[1,2], Karla Tapia[1], Selina Wu[1], Serim Yang[1,2], Xuefeng Ren[1,2], Roberto Zoncu[1,2] and James H. Hurley[1,2,3]

**Affiliations:**

[1]Department of Molecular and Cell Biology, University of California Berkeley; Berkeley CA 94720, USA.

[2]California Institute for Quantitative Biosciences, University of California, Berkeley, CA, 94720, USA

[3]Helen Wills Neuroscience Institute, University of California, Berkeley, Berkeley, CA 94720, USA

*Corresponding authors: rzoncu@berkeley.edu and jimhurley@berkeley.edu

**Abstract**

Mechanistic target of rapamycin complex 1 (mTORC1) is a nutrient-responsive master regulator of metabolism. Amino acids control the recruitment and activation of mTORC1 at the lysosome via the nucleotide loading state of the heterodimeric Rag GTPases. Under low nutrients, including arginine (Arg), the GTPase activating protein (GAP) complex, GATOR1, promotes GTP hydrolysis on RagA/B, inactivating mTORC1. GATOR1 is regulated by the cage-like GATOR2 complex and cytosolic amino acid sensors. To understand how the Arg-sensor CASTOR1 binds to GATOR2 to disinhibit GATOR1 under low cytosolic Arg, we determined the cryo-EM structure of GATOR2 bound to CASTOR1 in the absence of Arg. Two MIOS WD40 domain β-propellers of the GATOR2 cage engage with both subunits of a single CASTOR1 homodimer. Each propeller binds to a negatively charged MIOS-binding interface on CASTOR1 that is distal to the Arg pocket. The structure shows how Arg-triggered loop ordering in CASTOR1 blocks the MIOS-binding interface, switches off its binding to GATOR2, and so communicates to downstream mTORC1 activation.

**Main Text:**

mTORC1 is a master integrator of cell-extrinsic signaling and cell-intrinsic nutrient sensing, and a master regulator of the cellular balance between anabolism and catabolism[1-4]. As such, dysregulation of mTORC1 activity contributes to numerous cancers and metabolic disorders, making mTOR inhibitors a promising therapeutic strategy[5]. The key step in the activation of mTORC1 is its nutrient-regulated recruitment to the lysosomal membrane by the active Rag GTPase-Ragulator complex[6,7]. The Rag-Ragulator complex is composed of RagA or B GTPase, heterodimerized to RagC or D, and tethered to the membrane by the pentameric Ragulator/LAMTOR, whose LAMTOR1 subunit is lipidated[6,8]. In response to nutrients, including Arg, leucine (Leu), glucose and cholesterol, the Rags convert between two stable nucleotide states, inactive (RagA or $B^{GDP}$:RagC or $D^{GTP}$) and active (RagA or $B^{GTP}$:RagC or $D^{GDP}$)[9-12]. The active Rag dimer is responsible for recruiting mTORC1 to lysosomes[13-16]. When cytosolic amino acid levels are low, the Rag-Ragulator complex is inactivated by the GTPase activating protein (GAP) GATOR1, which promotes GTP-to-GDP hydrolysis by RagA/B[13]. The activity of GATOR1 is in turn regulated by the protein complexes GATOR2 and KICSTOR[13,17]. The entire system is targeted to the lysosome principally by the Rag-Ragulator complex[18]. GATOR1, GATOR2, and KICSTOR are not known to directly sense amino acids. Rather, a series of dedicated amino acid sensors that include CASTOR1, Sestrin2 and SAMTOR relay information about amino acids into the pathway by altering the activity of the GATOR1-GATOR2-KICSTOR complexes[19-21]. Understanding how such information is relayed at the structural level is a preeminent question in the regulation of cell metabolism.

GATOR2, a negative regulator of GATOR1, consists of five subunits, WDR59, WDR24, SEH1L, SEC13, and MIOS[13], that come together to form a higher order cage-like structure that

64 is membrane-less, and shares components and architectural elements with the COP-II cage and
65 the nuclear pore complex[22]. In their apo-states that occur under low amino acids, the Arg sensor
66 CASTOR1 and the Leu sensor Sestrin2 directly bind to GATOR2, preventing the latter from
67 inhibiting the GAP activity of GATOR1[19,20,22]. The CASTOR1 interaction with arginine triggers
68 the dissociation of CASTOR1 from GATOR2, though the structural mechanism for this step is
69 not yet understood[23]. Previous structural studies have uncovered the architecture of GATOR2
70 and individual nutrient sensors[22-27]. Here, we report the structure of GATOR2 in complex with
71 CASTOR1 in the absence of Arg. By comparing this complex to the pre-existing structures of
72 CASTOR1 in the presence and absence of Arg, we were able to deduce and validate the
73 mechanism whereby Arg binding triggers the release of CASTOR1 from GATOR2 by
74 modulating the conformation of a MIOS-releasing loop and so regulating the accessibilty of the
75 MIOS binding interface of CASTOR1.
76
77 **Cryo-EM Structure of the GATOR2-CASTOR1 Complex**
78 To isolate a stable GATOR2-CASTOR1 complex, we purified wild-type GATOR2 from
79 HEK 293 cells co-transfected with WDR59, WDR24, SEH1L, SEC13, and MIOS. We separately
80 purified a mutant apo-locked CASTOR1$^{S111A/D304A}$ (ref.[23]; hereafter referred to as
81 "CASTOR1$^{apo}$") from an *E. coli* expression system (Extended Data Fig. 1). The purified
82 GATOR2 and CASTOR1$^{apo}$ were combined, and the cryo-EM structure of GATOR2 bound to
83 CASTOR1$^{apo}$ was determined to an overall resolution of 3.89 Å (Fig. 1 and Extended Data Fig.
84 2). The resolution of the complex was further improved through local refinement resulting in a
85 resolution range of 3.02 Å - 3.72 Å (Extended Data Fig. 3 and Extended Data Fig. 4). The cryo-
86 EM density was of sufficient quality to generate an atomistic model of the ordered portions of

87 the core cage of GATOR2 and CASTOR1$^{apo}$ (Fig. 1 and Extended Data Fig. 5). The resulting
88 dimensions for the GATOR2-CASTOR1$^{apo}$ complex (hereafter simply "GATOR2-CASTOR1")
89 were 207 Å x 235 Å x 137 Å. The C2 symmetry of the GATOR2 complex is broken upon
90 CASTOR1 engagement. Analysis of the refined coordinates revealed that the C2 symmetry of
91 the unbound GATOR2 cage is broken in CASTOR1-bound complex (Extended Data Fig. 6),
92 although the two asymmetric units differ by only 1.2 Å r.m.s.d. for Cα atoms.
93 As seen in the absence of CASTOR1, GATOR2 assembles into an octagonal scaffold
94 containing four copies of MIOS, two copies of WDR24, two copies of WDR59, two copies of
95 SEC13, and six copies SEH1L[22]. The scaffold is stabilized by four zinc-binding C-terminal
96 domains (CTD) junctions, two of which are formed MIOS-WDR24 and two by MIOS-WDR59,
97 and four junctions formed by interactions between the α-solenoid domains of MIOS-MIOS and
98 WDR24-WDR59[22] (Fig. 2a). The two MIOS subunits straddling the 'front' face of GATOR2
99 engage the CASTOR1 homodimer (Fig. 1), while the other two back-facing MIOS β-propellers
100 that do not engage CASTOR1 are disordered and are not seen in the final density map and
101 reconstruction (Fig. 1 and 2a).
102
103 **CASTOR1 triggers structural rearrangements in GATOR2**
104 The MIOS subunits in GATOR2 play an integral role in the organization of the overall
105 complex core. Comparison with the GATOR2$^{apo}$ unbound structure shows that engagement of
106 CASTOR1 with the front face MIOS β-propellers triggers conformational changes throughout
107 the GATOR2 structure (Fig 2a and 2b, Extended Data Movie 1). Specifically, upon interaction
108 with CASTOR1, the front face MIOS β-propeller pair break their internal interface, pushing
109 apart 10 Å apart and rotating by 16 degrees relative to the MIOS α-solenoid domains of the inner

110 core of the GATOR2 cage (Fig. 2a and 2b) In the GATOR2 unbound conformation, the MIOS
111 interface responsible for interaction with CASTOR1 is exposed and not buried in the β-propeller
112 interface. However, the MIOS β-propellers are too close together to engage both CASTOR1
113 monomers simultaneously, and thus must reorient in the bound conformation. The back face
114 MIOS β-propellers, in contrast, are already separated by a 20 Å gap in unbound GATOR2 [22] (Fig
115 2b). This gap is too far apart to engage the CASTOR1 dimer and therefore they do not interact
116 with CASTOR1 in the bound complex (Fig. 2b).

117 The MIOS subunits are intimately linked with the WDR59 subunits through the MIOS-
118 WDR59 CTD junctions in the GATOR2 complex (Extended Data Fig. 7a). In the GATOR2-
119 CASTOR1 complex, the MIOS β-propeller reorientation pushes the front face SEH1L$^{MIOS}$
120 subunits outward ~8 Å and shifts the MIOS solenoidal and CTD domains. Compared to
121 GATOR2$^{apo}$, this movement in the front face MIOS solenoidal and CTD domains results in the
122 disordering of residues 757-836 and 890-921 in WDR59 and residues 727-746 and 770-783 in
123 MIOS (Extended Data Fig. 7b). These residues include the zinc finger (ZnF) motif in MIOS and
124 WDR59 (Extended Data Fig. 7b). In the GATOR2$^{apo}$ unbound structure, the ZnF, along with the
125 RING domains in MIOS and WDR59 stabilize the CTD-CTD junctions. Specifically, the MIOS
126 ZnF interacts with Sec13 and the WDR59 ZnF interact with SEH1L[22]. The ZnF contacts are no
127 longer present in the CASTOR1 bound state. However, the RING domains remain intact,
128 preserving the integrity of the GATOR2 cage (Extended Data Fig. 7a).

129

130 **The CASTOR1:GATOR2 interface**

131 In the GATOR2 bound structure, a single CASTOR1$^{apo}$ homodimer binds across one face
132 of the GATOR2 cage, engaging one MIOS β-propeller domain per CASTOR1$^{apo}$ monomer (Fig.

133 3a and 3b). The organization of the GATOR2-bound CASTOR1$^{apo}$ dimer is unaltered as
134 compared to the previous CASTOR1$^{apo}$ crystal structure[27]. The CASTOR1$^{apo}$ bound to GATOR2
135 and the isolated CASTOR1$^{apo}$ crystal structure only differ by 0.7Å rmsd for Cα atoms. Each
136 CASTOR1monomer of consists of four ACT (aspartate kinase, chorismate mutase and TyrA)
137 domains that interact through the interface composed of the ACT1 and ACT4 domains[23,25,26].
138 The two CASTOR1 monomers in the GATOR2-bound CASTOR1 dimer remain equivalent and
139 the two MIOS binding interfaces as defined by cryo-EM (Fig. 3a) are essentially superimposable
140 on one another. Each interface buries 690 Å$^2$ of solvent accessible surface area.
141
142 Two MIOS loops are responsible for most of the contacts with CASTOR1$^{apo}$ (Fig. 3b and
143 3c). Loop #1 (residues 110-114) is located between blade 2 and 3 in the MIOS β-propeller, while
144 loop #2 (residues 134-140) connects two β-sheets in blade 3 (Fig. 3c). The MIOS loop contacts
145 are centered on the basic residues His112, His136, and Arg137, with Lys135 at the edge of the
146 contact region (Fig. 3d-f). These four basic residues engage with a complementary
147 electronegative pocket on the surface of CASTOR1$^{apo}$ centered on Asp121 and also containing
148 Tyr118, Gln119, and Tyr236 (Fig. 3f). To validate the role of the MIOS binding interface in Arg
149 sensing, mutants were generated within the CASTOR1 pocket (D121A, Y118A, Q119A and
150 W236A) and on the two MIOS loops (H112A, K135A, H136A, R137A). The CASTOR1
151 residues Asp121, Tyr118 and Gln119 and MIOS residue R137 were previously noted to be
152 important for GATOR2 interaction[23,28]. We transiently expressed WT (FLAG-tagged)
153 CASTOR1, or CASTOR1 containing single mutation Y118A, Q119A, D121A or Y236A in
154 HEK-293T cells. As previously reported, in Arg-deprived cells WT CASTOR1-FLAG interacted
155 strongly with endogenous GATOR2 (revealed by immunoblotting for MIOS and WDR59), and

156 this interaction was weakened by Arg refeeding[10] (Fig. 3g). The interaction between GATOR2
157 and CASTOR1 was disrupted in cells expressing mutants within the core of the MIOS binding
158 interface on CASTOR1, Y118A and Q119A and D121 as well as cells expressing the mutant
159 Y236A on the periphery of the MIOS binding interface (Fig. 3g). Next, we co-expressed WT
160 MIOS-FLAG or MIOS-FLAG MIOS binding interface mutants (H112A, K135A, H136A and
161 R137A) with WT CASTOR1-HA in HEK-239T cells. Mutations in MIOS loop #1 (H112A) and
162 loop #2 (H136A and R137A) that are central to the MIOS binding interface disrupted GATOR2
163 interaction with CASTOR1 (Fig. 3h). Mutating a MIOS residue on the periphery of the MIOS
164 binding interface (K135A) has no noticeable effect as compared to WT in Arg-starved
165 conditions. However, the R135A MIOS mutant underwent a more complete dissociation from
166 CASTOR1-HA than the WT protein upon Arg supplementation, suggesting partial
167 destabilization of the interaction with CASTOR1 by this mutation (Fig. 3h). These data validate
168 the functional relevance of both sides of the CASTOR1-MIOS interface.
169 To understand the role of the CASTOR1-MIOS interaction on downstream mTORC1
170 activity, we monitored the phosphorylation of the mTORC1 substrate S6K1 in HEK-293T cells
171 depleted for endogenous CASTOR1 via shRNA-mediated knockdown, and reconstituted with
172 transiently expressing CASTOR1, or CASTOR1 containing single mutation Y118A, Q119A,
173 D121A or Y236A. Depletion of endogenous CASTOR1 rendered mTORC1 partially resistant to
174 Arg deprivation, as shown by enhanced phosphorylation of HA-tagged S6K1 in the Arg-depleted
175 sample (Fig. 3i). Co-expressing WT CASTOR1-FLAG restored the suppression of HA-S6K1
176 phosphorylation by Arg depletion. In contrast to WT, and consistent with their inability to bind
177 to GATOR2, the Y118A, Q119A, D121 and Y236A CASTOR1 mutants failed to restore the
178 normal pattern of HA-S6K1 phosphorylation by Arg (Fig. 3i).

179

180 **Mechanism of Arginine-induced CASTOR1 dissociation from GATOR2**

181 The MIOS binding interface on CASTOR1$^{apo}$ is located distal to the Arg binding pocket
182 (Fig. 4a). To understand how information about Arg levels is communicated between the Arg
183 binding pocket and MIOS binding interface, we compared the CASTOR1$^{apo}$ structure obtained
184 through the complex of GATOR2-CASTOR to the crystal structure of CASTOR1 bound to
185 arginine [23] (PDB:5I2C) (hereafter referred to as CASTOR1$^{Arg}$) as overlaid on the GATOR2
186 complex. Examining the electrostatic surface pattern of CASTOR1$^{apo}$ and CASTOR1$^{Arg}$ revealed
187 that only CASTOR1$^{apo}$ has an intact MIOS binding interface for interaction with MIOS (Fig.4b
188 and 4c). We term the CASTOR1 loop consisting of residues 86-94, which connects β6 and α3 of
189 the ACT2 domain, as the MIOS releasing loop. In CASTOR1$^{apo}$, the MIOS releasing loop is
190 disordered, which exposes the negatively charged MIOS binding interface residues Tyr118,
191 Gln119, Asp121 and Tyr236 (Fig. 4b). In the CASTOR1$^{Arg}$ structure, the residues 90-94 in the
192 MRL are ordered, cover the MIOS binding interface, and sterically block the MIOS-CASTOR1
193 interaction (Fig. 4c). In essence, the MIOS releasing loop acts as a lid for the MIOS binding
194 interface (Fig. 4a). Disordering of the MIOS releasing loop was previously seen in the isolated
195 CASTOR1$^{apo}$ crystal structure, however, the functional and mechanistic relevance of these
196 residues was not explored[27].

197 To test our structural hypothesis that the MIOS releasing loop is responsible for
198 dissociating CASTOR1 from MIOS upon Arg binding, we replaced the MIOS releasing loop
199 with a poly-Gly segment of equal length, CASTOR1$^{86-94G}$, which was designed to be disordered
200 constitutively. The structural hypothesis predicts that the MIOS binding interface of
201 CASTOR1$^{86-94G}$ would remain exposed and functional for MIOS binding even in the presence of

202 Arg. Consistent with the prediction, in HEK293T cells, overexpression of the CASTOR1$^{86\text{-}94G}$
203 mutant constitutively bound to MIOS and suppressed mTORC1 phosphorylation of S6K
204 irrespective of Arg levels (Fig. 4d and 4e).

205 To explain at the structural level how the negatively charged pocket in CASTOR1$^{apo}$ is
206 linked to binding of arginine in the arginine binding pocket on the other side of CASTOR1, we
207 overlayed the CASTOR1$^{apo}$ and CASTOR1$^{Arg}$ structures. The global architecture of the proteins
208 remained similar, with rotations observed in the α-helices in the ACT2 and ACT4 domains, the
209 portion of CASTOR1 that consists of the arginine binding pocket (Fig. 4f-h). The structural
210 comparison shows how adjustments in the ACT2 and 4 domains can transmit the Arg signal
211 from the Arg pocket on one side of the CASTOR1 monomer to the MIOS releasing loop on the
212 other side of the protein.

213

214 **GATOR2 interaction with CASTOR1 and Sestrin2**

215 The leucine sensor, Sestrin2, works in parallel with CASTOR1 to inhibit the activity of
216 GATOR2 and activate GATOR1[9,19] when cellular amino acid levels are low. The cryo-EM
217 structure of GATOR2-CASTOR revealed the proposed binding sites for Sestrin2 and GATOR1
218 on WDR24 and WDR59, respectively, remained free. To visualize how CASTOR1 and Sestrin2
219 simultaneously engages with the GATOR2, we purified WT GATOR2, WT GATOR1,
220 CASTOR1$^{apo}$ and a mutant apo-locked Sestrin2$^{E451Q/R390A/W444E}$ (ref.[23,24]; hereafter referred to as
221 "Sestrin2$^{apo}$") from an *E. coli* expression system (Extended Data Fig. 1) to generate a cryo-EM
222 sample of GATOR2, GATOR1, Sestrin2 and CASTOR1.

223 A density map was generated for the complex of GATOR2-CASTOR1-Sestrin2
224 (Extended Data Fig. 8a-d). GATOR1 present in the sample and was visualized in the data

225 processing but was not detected bound to the GATOR2-CASTOR1-Sestrin2 complex (Extended
226 Data Fig. 8e). GATOR2-CASTOR1$^{apo}$ docked into the final map suggesting Sestrin2 was
227 compatible with the GATOR2- CASTOR1$^{apo}$ cage alterations (Extended Data Fig 9a).
228 Unassigned density was visible in the map at the location of the WDR24 β-propeller and
229 adjacent to it (Extended Data Fig 9a). We generated an AlphaFold model of Sestrin2 with a
230 portion of one GATOR2 asymmetric unit containing one copy of WDR24, two copies of SEH1L
231 and one copy of MIOS (Extended Data Fig. 9c). The AlphaFold model was fitted in the cryo-EM
232 map through alignment with the SEH1L subunit connected to WDR24 in GATOR2-CASTOR1
233 (Extended Data Fig. 9b). In the AlphaFold model, Sestrin2 makes significant contact with the
234 WDR24 β-propeller, as suggested by previous studies[24,28], burying 1,195 Å$^2$ of surface area. The
235 interface in the AlphaFold model was analyzed and WDR24 Arg228 made critical contacts with
236 the negatively charged Sestrin2 surface (Extended Data Fig. 9d and 9e). To validate this
237 interaction, a mutant was generated in the WDR24 β-propeller (R228D). We transiently
238 expressed WT HA-tagged Sesrin2 along with WT FLAG-tagged WDR24, or WDR24 containing
239 single mutation R228D in HEK-293T cells.
240
241 As previously reported, in Leu-deprived cells WT HA-Sestrin2 interacted strongly with
242 the GATOR2 subunit WDR24, and this interaction was weakened by Leu refeeding[10] (Extended
243 Data Fig. 9f). The interaction between GATOR2 and Sestrin2 was disrupted in cells expressing
244 WDR24 R228D suggesting the relevance of the interface observed in the AlphaFold model
245 (Extended Data Fig. 9f). Our cryo-EM and AlphaFold model revealed the location of Sestrin2
246 binding that is compatible with CASTOR1 interaction with GATOR2. While we only observed
247 one stably bound copy of Sestrin2 via cryo-EM, it remains possible that an additional copy of

248 Sestrin2 could interact with the cage given the second copy of WDR24. Together, these data
249 show that Sestrin2 and CASTOR1 bind to the same conformational state of GATOR2, consistent
250 with a common mechanism for downstream regulation of GATOR1.
251
252 **Discussion**
253
254 The new structure presented here is consistent with a model that links CASTOR1
255 interaction with Arg to changes in the GATOR2-CASTOR1 interaction, and reveals a
256 mechanism for Arg-induced dissociation of CASTOR1 from GATOR2 leading to mTORC1
257 activation. Here, we directly visualized the CASTOR1 MIOS-binding interface. Previous
258 structural comparison of isolated apo- and arginine-bound CASTOR1 crystal structures noted
259 two missing loop regions in the apo-CASTOR1 structure [27]. The functional implications of this
260 change had been unclear, but can now be understood in light of the structure of the GATOR2-
261 CASTOR1 complex. The Arg binding pocket and the MIOS binding interface reside on opposite
262 faces of CASTOR1, and are connected by the α-helices of the ACT2 and ACT4 domains. In low
263 Arg conditions, the GATOR2 pocket is exposed while the arginine binding pocket is covered.
264 Upon increases in Arg levels, Arg enters the binding pocket and signals through conformational
265 changes in the α-helices to the opposite face of CASTOR1. This leads to ordering of the MIOS
266 releasing loop, occlusion of the MIOS binding interface, and so to the release of CASTOR1 from
267 GATOR2 (Fig. 4i).
268 We found that one CASTOR1 dimer engages two MIOS WD40 domains on the front
269 face of GATOR2 even though two other MIOS subunits are present on the back face of the cage.
270 The inability of CASTOR1 to bind to the back face MIOS dimer is explained by the greater
271 separation of these domains. At 20 Å apart in the unbound GATOR2 structure, it may be
272 sterically impossible to draw the back face MIOS β-propeller pair together to the 10 Å separation

273 needed to bind the CASTOR1 dimer. This prevents the formation of a 2:4 GATOR2 asymmetric
274 unit:CASTOR1 monomer complex. Thus, while the overall cage remains intact, conformational
275 changes extend over the entire cage and break exact C2 symmetry.

276 The critical remaining question is how the Arg signal is transduced to GATOR1. In yeast,
277 the counterparts of GATOR1 and 2 (the SEA complex) interact directly. The cryo-EM structure
278 of the SEA has been determined[29], yet the precise mechanism of GATOR1 GAP regulation is
279 still unclear, even in yeast. A third protein complex, KICSTOR, is present in mammals that does
280 not exist in yeast[17]. KICSTOR has been shown to engage both GATOR1 and GATOR2 and
281 regulate their activity[17,30]. The structure of the GATOR2-CASTOR1-Sestrin2 triple complex
282 determined here shows that these factors can bind simultaneously, a result consistent with the
283 expectation that, physiologically, low-nutrient states should involve simultaneous depletion of
284 multiple amino acid species. Now that the key question as to how amino acid binding regulates
285 sensor engagement has been answered, at least for CASTOR1 and Arg, the central question
286 going forward is how GATOR1 GAP activity is regulated by the combined action of GATOR2-
287 CASTOR1-Sestrin2 and KICSTOR. GATOR2 interactions with Sestrin2, CASTOR1, and
288 GATOR1 are not mutually exclusive, and the findings here thus set the stage to ultimately
289 answer this question.

290 How the Rag GTPases interconvert between the active and inactive nucleotide states[9-12] is
291 at the very heart of understanding nutrient regulation of mTORC1. The nucleotide state of
292 RagC/D is important primarily for regulation of non-canonical mTORC1 substrates, of which the
293 MiT-TFE transcription factors are the best characterized [31]. The structural pathway for regulation
294 of the RagC/D nucleotide state by the FLCN-FNIP GAP complex has been worked out in large
295 part[32-35]. In contrast, despite its critical importance for both canonical and non-canonical

296 mTORC1 signaling, regulation of the nucleotide state of RagA/B remains incompletely
297 understood. Structural analysis of the GATOR1 GAP complex[36,37] and GATOR2[22] is making
298 strides towards a full structural and mechanistic explanation of this central event. The work
299 presented here adds another important piece to the puzzle, bringing us that much closer to a
300 complete structural view of how the RagA/B branch of mTORC1 signaling is regulated.
301

302

303 **Main References**

304


305 1 Ballabio, A. & Bonifacino, J. S. Lysosomes as dynamic regulators of cell and organismal
306 homeostasis. *Nat Rev Mol Cell Biol* **21**, 101-118 (2020). https://doi.org:10.1038/s41580-
307 019-0185-4
308 2 Goul, C., Peruzzo, R. & Zoncu, R. The molecular basis of nutrient sensing and signalling
309 by mTORC1 in metabolism regulation and disease. *Nat Rev Mol Cell Biol* **24**, 857-875
310 (2023). https://doi.org:10.1038/s41580-023-00641-8
311 3 Condon, K. J. & Sabatini, D. M. Nutrient regulation of mTORC1 at a glance. *J Cell Sci*
312 **132** (2019). https://doi.org:10.1242/jcs.222570
313 4 Battaglioni, S., Benjamin, D., Walchli, M., Maier, T. & Hall, M. N. mTOR substrate
314 phosphorylation in growth control. *Cell* **185**, 1814-1836 (2022).
315 https://doi.org:10.1016/j.cell.2022.04.013
316 5 Chiarini, F., Evangelisti, C., McCubrey, J. A. & Martelli, A. M. Current treatment
317 strategies for inhibiting mTOR in cancer. *Trends Pharmacol Sci* **36**, 124-135 (2015).
318 https://doi.org:10.1016/j.tips.2014.11.004
319 6 Sancak, Y. *et al.* Ragulator-Rag complex targets mTORC1 to the lysosomal surface and
320 is necessary for its activation by amino acids. *Cell* **141**, 290-303 (2010).
321 https://doi.org:10.1016/j.cell.2010.02.024
322 7 Sancak, Y. *et al.* The Rag GTPases bind raptor and mediate amino acid signaling to
323 mTORC1. *Science* **320**, 1496-1501 (2008). https://doi.org:10.1126/science.1157535
324 8 Sekiguchi, T., Hirose, E., Nakashima, N., Ii, M. & Nishimoto, T. Novel G proteins, Rag
325 C and Rag D, interact with GTP-binding proteins, Rag A and Rag B. *J Biol Chem* **276**,
326 7246-7257 (2001). https://doi.org:10.1074/jbc.M004389200
327 9 Wolfson, R. L. *et al.* Sestrin2 is a leucine sensor for the mTORC1 pathway. *Science* **351**,
328 43-48 (2016). https://doi.org:10.1126/science.aab2674
329 10 Chantranupong, L. *et al.* The CASTOR Proteins Are Arginine Sensors for the mTORC1
330 Pathway. *Cell* **165**, 153-164 (2016). https://doi.org:10.1016/j.cell.2016.02.035
331 11 Orozco, J. M. *et al.* Dihydroxyacetone phosphate signals glucose availability to
332 mTORC1. *Nat Metab* **2**, 893-901 (2020). https://doi.org:10.1038/s42255-020-0250-5
333 12 Shin, H. R. *et al.* Lysosomal GPCR-like protein LYCHOS signals cholesterol sufficiency
334 to mTORC1. *Science*, eabg6621 (2022). https://doi.org:10.1126/science.abg6621
335 13 Bar-Peled, L. *et al.* A Tumor suppressor complex with GAP activity for the Rag GTPases
336 that signal amino acid sufficiency to mTORC1. *Science* **340**, 1100-1106 (2013).
337 https://doi.org:10.1126/science.1232044
338 14 Rogala, K. B. *et al.* Structural basis for the docking of mTORC1 on the lysosomal
339 surface. *Science* **366**, 468-475 (2019). https://doi.org:10.1126/science.aay0166
340 15 Anandapadamanaban, M. *et al.* Architecture of human Rag GTPase heterodimers and
341 their complex with mTORC1. *Science* **366**, 203-210 (2019).
342 https://doi.org:10.1126/science.aax3939
343 16 Cui, Z. *et al.* Structure of the lysosomal mTORC1-TFEB-Rag-Ragulator megacomplex.
344 *Nature* **614**, 572-579 (2023). https://doi.org:10.1038/s41586-022-05652-7

17 Wolfson, R. L. *et al.* KICSTOR recruits GATOR1 to the lysosome and is necessary for nutrients to regulate mTORC1. *Nature* **543**, 438-442 (2017). https://doi.org:10.1038/nature21423

18 Valenstein, M. L. *et al.* Rag-Ragulator is the central organizer of the physical architecture of the mTORC1 nutrient-sensing pathway. *Proc Natl Acad Sci U S A* **121**, e2322755121 (2024). https://doi.org:10.1073/pnas.2322755121

19 Chantranupong, L. *et al.* The Sestrins interact with GATOR2 to negatively regulate the amino-acid-sensing pathway upstream of mTORC1. *Cell Rep* **9**, 1-8 (2014). https://doi.org:10.1016/j.celrep.2014.09.014

20 Chantranupong, L. *et al.* The CASTOR Proteins Are Arginine Sensors for the mTORC1 Pathway. *Cell* **165**, 153-164 (2016). https://doi.org:10.1016/j.cell.2016.02.035

21 Gu, X. *et al.* SAMTOR is an S-adenosylmethionine sensor for the mTORC1 pathway. *Science* **358**, 813-818 (2017). https://doi.org:10.1126/science.aao3265

22 Valenstein, M. L. *et al.* Structure of the nutrient-sensing hub GATOR2. *Nature* **607**, 610-616 (2022). https://doi.org:10.1038/s41586-022-04939-z

23 Saxton, R. A., Chantranupong, L., Knockenhauer, K. E., Schwartz, T. U. & Sabatini, D. M. Mechanism of arginine sensing by CASTOR1 upstream of mTORC1. *Nature* **536**, 229-233 (2016). https://doi.org:10.1038/nature19079

24 Saxton, R. A. *et al.* Structural basis for leucine sensing by the Sestrin2-mTORC1 pathway. *Science* **351**, 53-58 (2016). https://doi.org:10.1126/science.aad2087

25 Gai, Z. *et al.* Structural mechanism for the arginine sensing and regulation of CASTOR1 in the mTORC1 signaling pathway. *Cell Discov* **2**, 16051 (2016). https://doi.org:10.1038/celldisc.2016.51

26 Xia, J., Wang, R., Zhang, T. & Ding, J. Structural insight into the arginine-binding specificity of CASTOR1 in amino acid-dependent mTORC1 signaling. *Cell Discov* **2**, 16035 (2016). https://doi.org:10.1038/celldisc.2016.35

27 Zhou, Y., Wang, C., Xiao, Q. & Guo, L. Crystal structures of arginine sensor CASTOR1 in arginine-bound and ligand free states. *Biochem Biophys Res Commun* **508**, 387-391 (2019). https://doi.org:10.1016/j.bbrc.2018.11.147

28 Yang, C., Sun, X. & Wu, G. New insights into GATOR2-dependent interactions and its conformational changes in amino acid sensing. *Biosci Rep* **44** (2024). https://doi.org:10.1042/BSR20240038

29 Tafur, L. *et al.* Cryo-EM structure of the SEA complex. *Nature* **611**, 399-404 (2022). https://doi.org:10.1038/s41586-022-05370-0

30 Peng, M., Yin, N. & Li, M. O. SZT2 dictates GATOR control of mTORC1 signalling. *Nature* **543**, 433-437 (2017). https://doi.org:10.1038/nature21378

31 Napolitano, G., Di Malta, C. & Ballabio, A. Non-canonical mTORC1 signaling at the lysosome. *Trends Cell Biol* (2022). https://doi.org:10.1016/j.tcb.2022.04.012

32 Lawrence, R. E. *et al.* Structural mechanism of a Rag GTPase activation checkpoint by the lysosomal folliculin complex. *Science* **366**, 971-977 (2019). https://doi.org:10.1126/science.aax0364

33 Fromm, S. A., Lawrence, R. E. & Hurley, J. H. Structural mechanism for amino acid-dependent Rag GTPase nucleotide state switching by SLC38A9. *Nat Struct Mol Biol* **27**, 1017-1023 (2020). https://doi.org:10.1038/s41594-020-0490-9

389 34 Jansen, R. M. *et al.* Structural basis for FLCN RagC GAP activation in MiT-TFE
390 substrate-selective mTORC1 regulation. *Sci Adv* **8**, eadd2926 (2022).
391 https://doi.org:10.1126/sciadv.add2926
392 35 Cui, Z., Joiner, A. M. N., Jansen, R. M. & Hurley, J. H. Amino acid sensing and
393 lysosomal signaling complexes. *Curr Opin Struct Biol* **79**, 102544 (2023).
394 https://doi.org:10.1016/j.sbi.2023.102544
395 36 Shen, K. *et al.* Architecture of the human GATOR1 and GATOR1-Rag GTPases
396 complexes. *Nature* **556**, 64-69 (2018). https://doi.org:10.1038/nature26158
397 37 Egri, S. B. *et al.* Cryo-EM structures of the human GATOR1-Rag-Ragulator complex
398 reveal a spatial-constraint regulated GAP mechanism. *Mol Cell* (2022).
399 https://doi.org:10.1016/j.molcel.2022.03.002
400
401
402

403 **Figures**

404

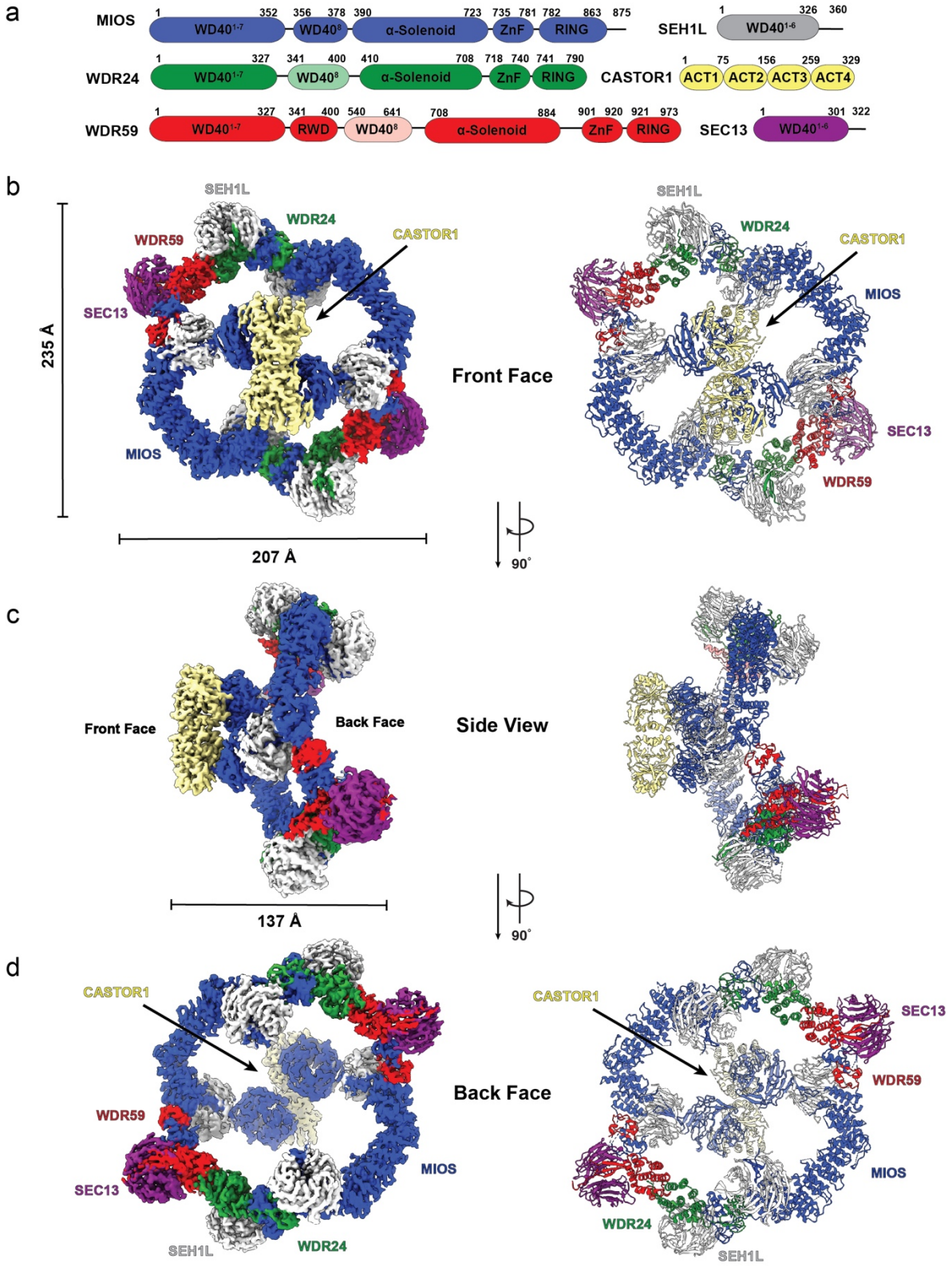


405

406 **Fig. 1: Cryo-EM structure of GATOR2-CASTOR1 complex.** (a) Domain organization of
407 subunits within the GATOR2-CASTOR1 structure. Composite map and reconstructed model for
408 the GATOR2-CASTOR1 complex viewing from the (b) front face (c) side view (d) back face.
409 Focused maps for different portions of the complex were combined to generate a composite map
410 containing the highest resolution information for each subunit.
411
412

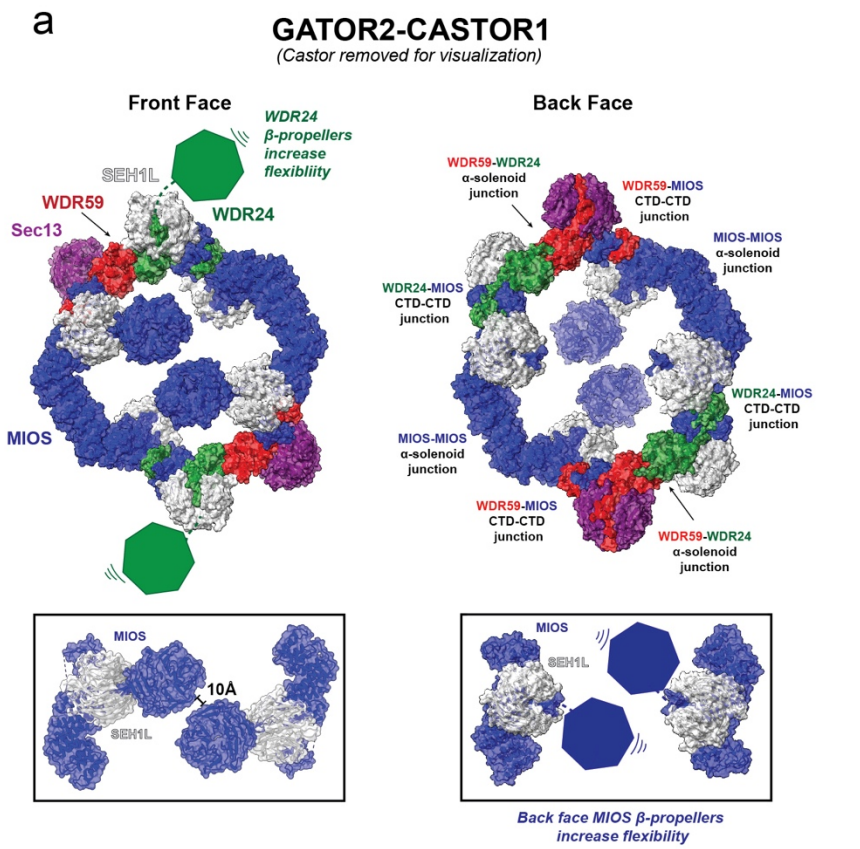
a
GATOR2-CASTOR1
(Castor removed for visualization)
Front Face
Back Face
WDR24
β-propellers
increase
flexibliity
SEH1L
WDR59
Sec13
WDR24
MIOS
WDR59-WDR24
α-solenoid
junction
WDR59-MIOS
CTD-CTD
junction
MIOS-MIOS
α-solenoid
junction
WDR24-MIOS
CTD-CTD
junction
WDR24-MIOS
CTD-CTD
junction
MIOS-MIOS
α-solenoid
junction
WDR59-MIOS
CTD-CTD
junction
WDR59-WDR24
α-solenoid
junction
MIOS
10Å
SEH1L
MIOS
SEH1L
Back face MIOS β-propellers
increase flexibility

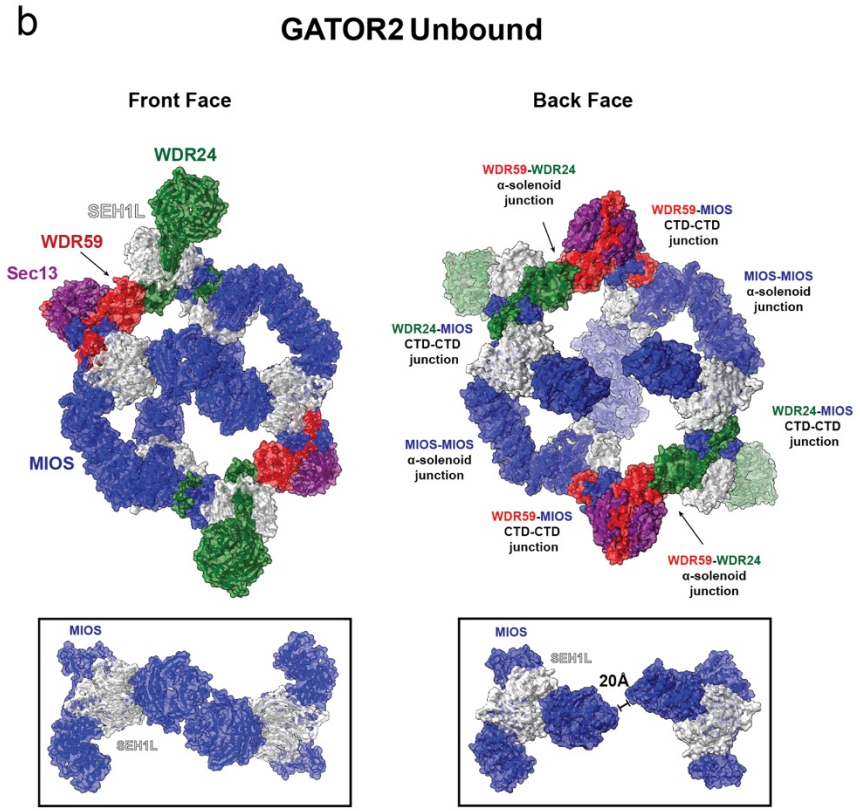
b
GATOR2 Unbound
Front Face
Back Face
WDR24
SEH1L
WDR59
Sec13
MIOS
WDR59-WDR24
α-solenoid
junction
WDR59-MIOS
CTD-CTD
junction
MIOS-MIOS
α-solenoid
junction
WDR24-MIOS
CTD-CTD
junction
WDR24-MIOS
CTD-CTD
junction
MIOS-MIOS
α-solenoid
junction
WDR59-MIOS
CTD-CTD
junction
WDR59-WDR24
α-solenoid
junction
MIOS
SEH1L
MIOS
SEH1L
20Å

413

414 **Fig. 2: CASTOR1 triggers a structural rearrangement in GATOR2 complex.** Comparison
415 of the front and back faces of the (a) GATOR2-CASTOR1 complex and (b) GATOR2$^{apo}$
416 complex. CASTOR1 is removed for visualization in the GATOR2-CASTOR1 complex. Changes
417 in the MIOS subunits are highlighted in boxes below complex. Key junctions connecting the
418 inner cage are indicated.
419

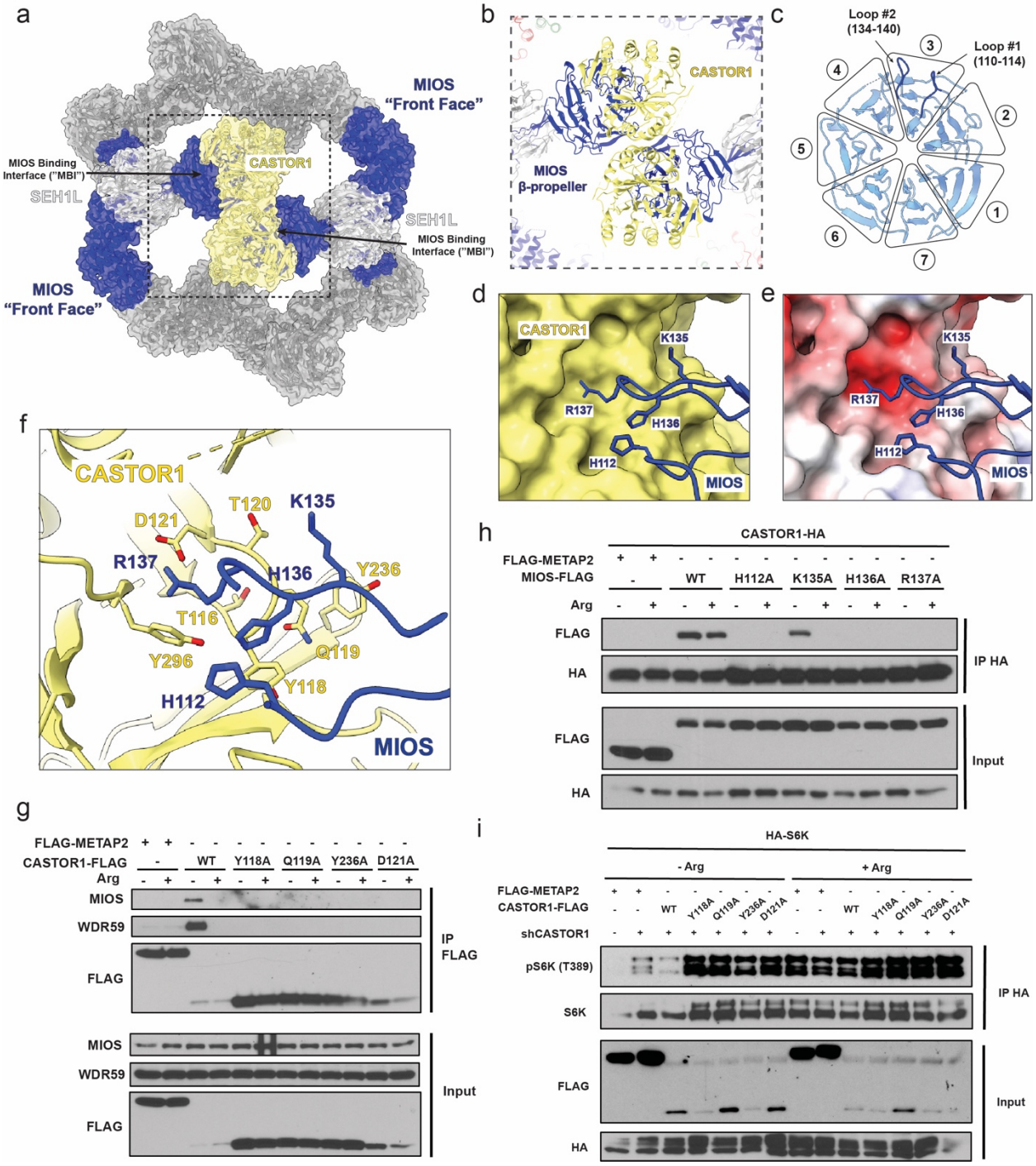


**Fig. 3: CASTOR1 interacts with MIOS through negatively charged pocket.** (a) Overview of GATOR2-CASTOR1 complex. Front face MIOS subunits (blue) interact with CASTOR1 (yellow). (b) Close up view of CASTOR1 interaction with MIOS β-propellers. (c) Blade diagram

425 for a front face MIOS β-propeller highlighting CASTOR1 interacting loops. Close up of the
426 CASTOR1-MIOS interaction shown with (d) CASTOR1 surface view and MIOS ribbon view (e)
427 CASTOR1 surface colored based on electrostatic potential (f) Ribbon view highlighting specific
428 residues in MIOS loops residues 110-114 and 134-140 (blue) interacting with CASTOR1
429 residues (yellow). (g) HEK-293T cells transiently expressing the indicated FLAG-tagged WT
430 and MIOS binding interface (MBI)-mutant CASTOR1 constructs, or FLAG-tagged METAP2 as
431 a control, were starved of arginine for 50 minutes and, where indicated, restimulated for 10
432 minutes. FLAG-immunoprecipitates were generated and analyzed by immunoblotting for the
433 indicated proteins. (h) HEK-293T cells transiently expressing CASTOR1-HA and either FLAG-
434 tagged WT MIOS, FLAG-tagged MBI-mutant MIOS constructs or FLAG-tagged METAP2 as a
435 control. Cells were starved of arginine for 50 minutes and, where indicated, restimulated for 10
436 minutes. HA-immunoprecipitates were generated and analyzed by immunoblotting for the
437 indicated proteins. (i) CASTOR1 knockdown HEK-293T cells transiently expressing the
438 indicated FLAG-tagged WT and MBI-mutant CASTOR1 constructs, or FLAG-tagged METAP2
439 as a control, were starved of arginine for 50 minutes and, where indicated, restimulated for 10
440 minutes. Anti-HA-immunoprecipitates were prepared and analyzed by immunoblotting for the
441 indicated proteins and phospho-proteins.
442

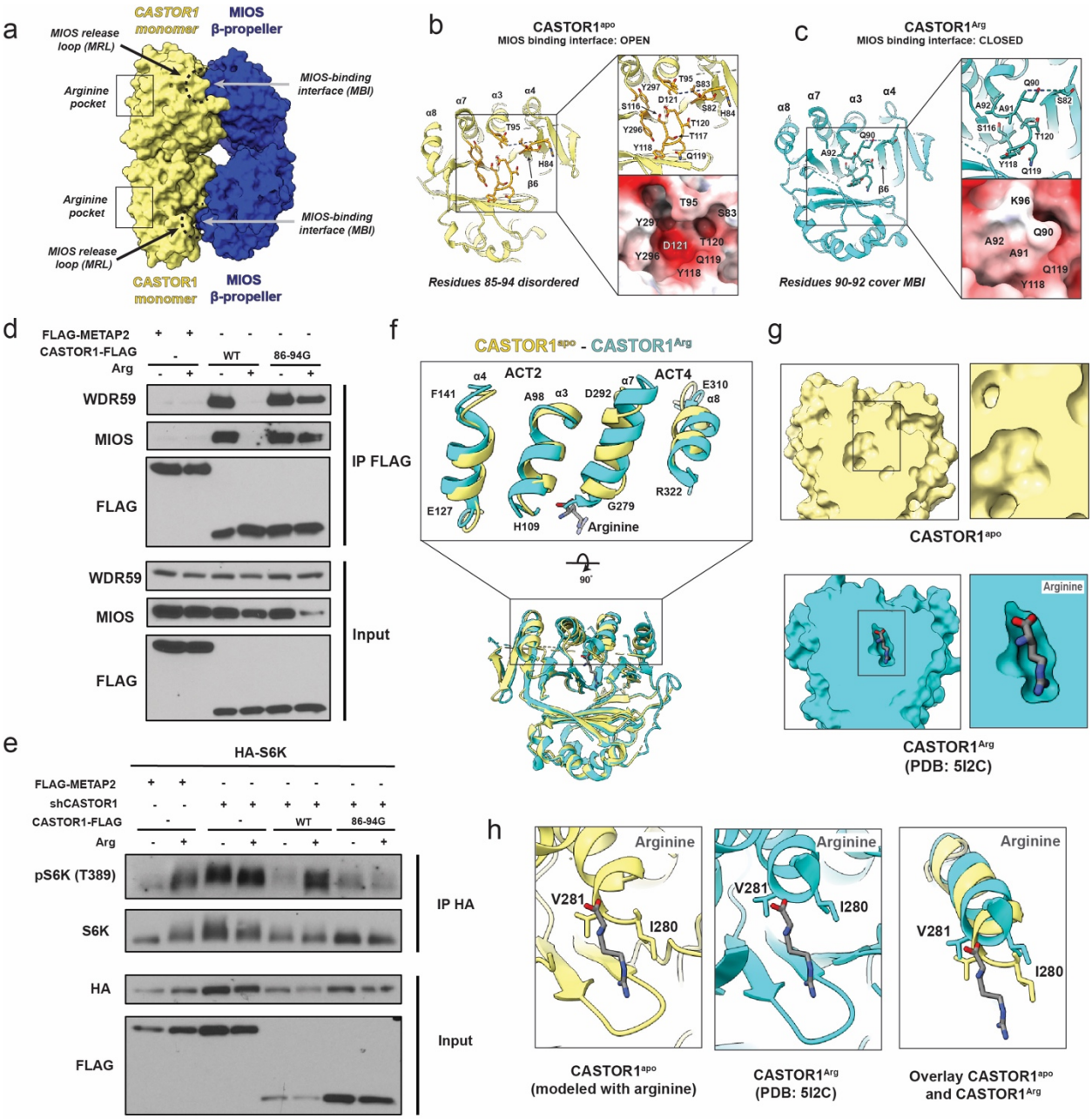
a
CASTOR1 monomer
MIOS β-propeller
MIOS release loop (MRL)
Arginine pocket
MIOS-binding interface (MBI)
Arginine pocket
MIOS-binding interface (MBI)
MIOS release loop (MRL)
CASTOR1 monomer
MIOS β-propeller
b
CASTOR1apo
MIOS binding interface: OPEN
Residues 85-94 disordered
c
CASTOR1Arg
MIOS binding interface: CLOSED
Residues 90-92 cover MBI
d
FLAG-METAP2
CASTOR1-FLAG
Arg
WT
86-94G
WDR59
MIOS
FLAG
IP FLAG
Input
e
HA-S6K
FLAG-METAP2
shCASTOR1
CASTOR1-FLAG
Arg
WT
86-94G
pS6K (T389)
S6K
HA
FLAG
IP HA
Input
f
CASTOR1apo - CASTOR1Arg
ACT2
ACT4
Arginine
90°
g
CASTOR1apo
Arginine
CASTOR1Arg
(PDB: 5I2C)
h
Arginine
V281
I280
CASTOR1apo
(modeled with arginine)
CASTOR1Arg
(PDB: 5I2C)
Overlay CASTOR1apo
and CASTOR1Arg
i
MRL MBI
ACTs
Arginine pocket
CASTOR1 MIOS
– Arg
MBI: Open
MRL: Disordered
+ Arg
MBI: Closed
MRL: Ordered
ACT2, ACT4
reorientation
Arginine

443

444 **Fig. 4: CASTOR1 interaction with arginine triggers closing of GATOR2-interacting**
445 **pocket.** (a) Diagram of CASTOR1 interaction with MIOS β-propellers and location of arginine
446 pocket and MIOS binding interface. (b) Electrostatic surface cartoon of CASTOR1$^{apo}$ and close
447 up of GATOR2-interact pocket. Key residues in CASTOR1 that form pocket are indicated. (c)
448 Electrostatic surface cartoon of CASTOR1$^{Arg}$ and close up of GATOR2-interact pocket. Key
449 residues in CASTOR1 that block pocket are indicated. (d) HEK-293T cells transiently
450 expressing the indicated FLAG-tagged WT and MIOS releasing loop (MRL)-mutant CASTOR1
451 constructs, or FLAG-tagged METAP2 as a control, were starved of arginine for 50 minutes and,
452 where indicated, restimulated for 10 minutes. FLAG-immunoprecipitates were generated and
453 analyzed by immunoblotting for the indicated proteins. (e) CASTOR1 knockdown HEK-293T
454 cells transiently expressing the indicated FLAG-tagged WT and MRL-mutant CASTOR1
455 constructs, or FLAG-tagged METAP2 as a control, were starved of arginine for 50 minutes and,
456 where indicated, restimulated for 10 minutes. Anti-HA-immunoprecipitates were prepared and
457 analyzed by immunoblotting for the indicated proteins and phospho-proteins. (f) Overlay of
458 CASTOR1$^{apo}$ (yellow) and CASTOR1$^{Arg}$ (cyan). Rotation in ACT2 and ACT4 α-helices enlarged
459 for visualization. (g) Surface view of CASTOR1$^{apo}$ and CASTOR1$^{Arg}$ arginine binding pocket.
460 CASTOR1$^{apo}$ is modelled with arginine in binding pocket. (h) Ribbon view of arginine binding
461 pocket in CASTOR1$^{apo}$ and CASTOR1$^{Arg}$. (i) Overall model for arginine-dependent CASTOR1
462 interaction with GATOR2.
463
464
465
466

467 **Methods**
468
469 Cloning and Protein Purification:

470 *GATOR2 purification*

471 Codon optimized DNA encoding all five subunits of GATOR2 (MIOS, WDR59,
472 WDR24, SEH1L and Sec13) was synthesized by Twist Biosciences and subcloned into the
473 pCAG vector. The construct with MIOS was engineering to include a N-terminal tandem-
474 STREP-FLAG tag. HEK293-GNTI cells were co-transfected with 1mg DNA with equal amount
475 of all five GATOR2 subunits and 4 mg P.E.I per 1L of cells at 2E6 cells/ml. Cells were
476 harvested after 48 hours and pelleted at 2000 xg for 20 min at 4 °C.

477 Cell pellets were resuspended in 30 mL lysis buffer (25 mM HEPES pH 7.5, 500 mM
478 NaCl, 2 mM $MgCl_2$, 10% glycerol, 1 mM TCEP, 1 protease inhibitor tablet (Roche) per 50 mL,
479 1 mM PMSF) and dounce homogenized prior to 1 hour incubation with 1% DDM:CHS (1:10) at
480 4 °C. The lysate was centrifuged at 37,000 xg for 35 minutes at 4 °C. The supernatant was
481 incubated with ~3-4 mL of Strep-Tactin Sepharose resin for 12-15 hours rocking at 4 °C. The
482 resin was washed with 20 mL high salt wash buffer A (25 mM HEPES, 500 mM NaCl, 2 mM
483 $MgCl_2$, 1 mM TCEP, 50 mM Arginine, 50 mM Glutamic Acid, 1 mM ATP, pH 7.4, 0.03%
484 DDM/CHS), 20 mL low salt wash buffer B (25 mM HEPES, 200 mM NaCl, 2 mM $MgCl_2$, 1
485 mM TCEP, 50 mM Arginine, 50 mM Glutamic Acid, 1 mM ATP, pH 7.4, 0.03% DDM/CHS),
486 20 mL low salt (no ATP) wash buffer C (25 mM HEPES, 200 mM NaCl, 2 mM $MgCl_2$, 1 mM
487 TCEP, 50 mM Arginine, 50 mM Glutamic Acid, pH 7.4, 0.03% DDM/CHS), and 20 mL low
488 salt (no ATP, no DDM:CHS) wash buffer D (25 mM HEPES, 200 mM NaCl, 2 mM $MgCl_2$, 1
489 mM TCEP, 50 mM Arginine, 50 mM Glutamic Acid, pH 7.4). GATOR2 was eluted from the
490 Strep-Tactin Sepharose resin using 20 mL elution buffer (25 mM HEPES, 200 mM NaCl, 2 mM

491 $MgCl_2$, 1 mM TCEP, 50 mM Arginine, 50 mM Glutamic acid, pH 7.4, 4mM desthiobiotin).
492 Eluted protein was concentrated to 1 mL using a Milipore Amicon Ultra Centrifugal Filter and
493 subjected to gel filtration using a Superose 6 Increase 10/300 and buffer containing 25 mM
494 HEPES, 200 mM NaCl, 2 mM $MgCl_2$, 1 mM TCEP.
495
496 *CASTOR1$^{apo}$ purification*
497 Codon optimized DNA encoding CASTOR1 S111A/D304A was synthesized by Twist
498 Biosciences and subcloned into the pET-28a+ vector containing an N-terminal 6X-His tag. The
499 vector containing 6X-His-CASTOR1$^{apo}$ was transformed into BL21(DE3) cells. Cells were
500 grown at 37 °C until the optical density (OD) reached 0.6. Protein production was induced using
501 0.2 mM IPTG at 18 °C for 14-16 hours. Cells were pelleted via centrifugation at 3500 xg for 20
502 minutes.
503 Cell pellets were resuspended in ~50 mL lysis buffer (30 mM Tris-HCL, 200 mM NaCl,
504 1mM TCEP, 1 mM PMSF) and lysed via sonication for 5 minutes, 2 seconds ON, 2 seconds
505 OFF. The lysate was centrifuged at 37,000 xg for 35 minutes at 4 °C. The supernatant was
506 incubated with ~3 mL HisPur Ni-NTA resin (Thermo Scientific) for 1-2 hr rocking at 4 °C. The
507 resin was washed with ~150 mL wash buffer (30 mM Tris-HCL, 200 mM NaCl, 30 mM
508 imidazole, 1mM TCEP) before elution with ~80 mL elution buffer (30 mM Tris-HCL, 200 mM
509 NaCl, 200 mM imidazole, 1mM TCEP). The protein was concentrated using Milipore Amicon
510 Ultra Centrifugation Filter to 1 mL. The concentrated protein was subjected to gel filtration using
511 HiLoad 16/600 Superdex 200 pg column and buffer containing (10mM HEPES, pH 7.5, 100mM
512 NaCl, 0.5mM TCEP).
513

514 *Sestrin2$^{apo}$ purification*

515 Codon optimized DNA encoding Sestrin2 E451Q/ R390A/ W444E was synthesized by
516 Twist Biosciences and subcloned into the pET-28a+ vector containing an N-terminal 6X-His tag.
517 The vector containing 6X-His-Sestrin2$^{apo}$ was transformed into BL21(DE3) cells. Cells were
518 grown at 37 °C until the optical density (OD) reached 0.7. Protein production was induced using
519 0.2 mM IPTG at 18 °C for 14-16 hours. Cells were pelleted via centrifugation at 3500 xg for 20
520 minutes.

521 Cell pellets were resuspended in ~50 mL lysis buffer (50mM Potassium Phosphate pH
522 8.0, 500mM NaCl, 30mM imidazole, 3mM BME, and 1mM PMSF) and lysed via sonication for
523 5 minutes, 2 seconds ON, 2 seconds OFF. The lysate was centrifuged at 37,000 xg for 35
524 minutes at 4 °C. The supernatant was passed through ~5 mL HisPur Ni-NTA resin (Thermo
525 Scientific) , collected and passed through 2x more. The resin was washed with ~150 mL wash
526 buffer (50mM Potassium Phosphate pH 8.0, 500mM NaCl, 30mM imidazole, 3mM BME, and
527 1mM PMSF) before elution with ~50 mL elution buffer (50mM Potassium Phosphate pH 8.0,
528 150mM NaCl, 250mM imidazole, 3mM BME). The protein was dialyzed using SnakeSkin
529 Dialysis Tubing (10K MWCO) (Thermo Scientific) in 4L of buffer containing 10mM potassium
530 phosphate and 100mM NaCl at 4 °C for 14-16 hours. The protein was passed through 5mL
531 HiTrap SP HP cation exchange column (Cytiva) and the flow through was collected and saved.
532 The protein was concentrated using Milipore Amicon Ultra Centrifugation Filter to 1 mL. The
533 concentrated protein was subjected to gel filtration using HiLoad 16/600 Superdex 200 pg
534 column and buffer containing (10mM Tris-HCl pH 8.0, 150mM NaCl, 0.1mM EDTA and
535 0.5mM TCEP).

536

537 *GATOR1 purification*

538 HEK293-GNTI cells were co-transfected with 1mg DNA encoding the GATOR1
539 subunits GST-tagged DEPDC5, NPRL2 and NPRL2 at a 1:2:2 ratio and 4 mg P.E.I per 1L of
540 cells at 2E6 cells/ml. Cells were harvested after 48 hours and pelleted at 2000 xg for 20 min at 4
541 °C. Cell pellets were resuspended in 30 mL lysis buffer (25 mM HEPES pH 7.5, 130 mM NaCl,
542 2.5 mM $MgCl_2$, 2mM EGTA, 1% Triton-X 0.5 mM TCEP, and 1 protease inhibitor tablet
543 (Roche) per 50 mL) and incubated for 1 hour at 4 °C. The lysate was centrifuged at 37,000 xg for
544 35 minutes at 4 °C. The supernatant was incubated with ~3-4 mL of Glutathione Sepharose resin
545 for 3 hours rocking at 4 °C. The resin was washed with 15 mL lysis buffer, 15 mL high salt lysis
546 buffer (25 mM HEPES pH 7.5, 500 mM NaCl, 2.5 mM $MgCl_2$, 2mM EGTA, 1% Triton-X 0.5
547 mM TCEP), 10mL lysis buffer and 15mL gel filtration buffer (25mM HEPES pH 7.5, 130mM
548 NaCl, 2.5mM $MgCl_2$, 0.5mM TCEP). The column was sealed and an additional 5mL of gel
549 filtration and TEV protease was added. The column was incubated with TEV protease overnight
550 for cleavage. The protein was eluted from the column with 15 mL gel filtration buffer and
551 concentrated to 1 mL using a Milipore Amicon Ultra Centrifugal Filter. The sample was
552 subjected to gel filtration using a Superose 6 Increase 10/300 for a final polishing step with
553 buffer containing 25 mM HEPES pH 7.5, 130 mM NaCl, 2 mM $MgCl_2$, 0.5 mM TCEP).

554

555 <u>Cryo-EM Grid Preparation and Imaging:</u>

556 *GATOR2-CASTOR1$^{apo}$*

557 Purified GATOR2 was concentrated to 0.45 mg/mL. 3-fold molar excess of CASTOR1
558 was added and incubated for 45 minutes on ice and immediately froze on grids. 3 µl sample was
559 deposited onto freshly glow-discharged (PELCO easiGlow, 30 s in air at 15 mA and 0.4 mbar)

560 holey carbon grids (C-flat: 2/1-3Cu-T). FEI Vitrobot Mark IV was used to blot grids for 3
561 seconds with a blot force of 20 (Whatman 597 filter paper) at 4℃ and 100 % humidity and
562 subsequentially plunged into liquid ethane. The Titan Krios G3i microscope equipped with a
563 Gatan Quantum energy filter (slit width 20 eV) and a K3 summit camera at a defocus of -1.0 to -
564 2.0 µm was used to record 11,950 movies. Automated image acquisition was performed using
565 SerialEM [1] recording four movies per 2 µm hole with image shift. Image parameters are
566 summarized in Extended Table 1.
567
568 *GATOR2-CASTOR1$^{apo}$- Sestrin2$^{apo}$ – GATOR1*
569 Purified GATOR2 was concentrated to 0.45 mg/mL. 3-fold molar excess of CASTOR1,
570 2-fold molar excess of Sestrin2, and 3-fold molar excess of GATOR1 was added and incubated
571 for 45 minutes on ice and immediately froze on grids. 3 µl sample was deposited onto freshly
572 glow-discharged (PELCO easiGlow, 30 s in air at 15 mA and 0.4 mbar) holey carbon grids (C-
573 flat: 2/1-3Cu-T). FEI Vitrobot Mark IV was used to blot grids for 3 seconds with a blot force of
574 20 (Whatman 597 filter paper) at 4℃ and 100 % humidity and subsequentially plunged into
575 liquid ethane. The Talos Arctica microscope equipped with a Gatan K3 camera at a defocus of -
576 1.0 to -2.0 µm was used to record 3,931 movies. Automated image acquisition was performed
577 using SerialEM [1] recording 2 movies per 2 µm hole with image shift. Image parameters are
578 summarized in Extended Table 1.
579
580 <u>Cryo-EM Data Processing:</u>
581 The data processing workflow for GATOR2-CASTOR1$^{apo}$ is summarized in Extended
582 Data Fig.1. In short, raw movies were imported into cryosparc2 v4.3.1 [2]. Patch Motion Corr. was

583 used for motion correction and Patch CTF estimated (multi) was used for CTF determination.
584 Cryosparc blob picker with a diameter range of 200Å-280Å was used to generate 3,467,659
585 which was inspected to trim the particle set to 2,289,288 particles. Particles were extracted with a
586 box size of 560x560 pixels in cryosparc2. A series of 2D classifications followed by an ab-initio-
587 reconstruction was used to generate three reference maps. The resulting 3D maps were used in
588 addition to maps generated from prior datasets to resort all 2,289,288 particles after a round of
589 2D classification to remove obvious 'junk'. The final particle set contained 140,606 particles and
590 a round of homogenous refinement resulted in a 3.89Å map at 0.143 FSC. Masks were generated
591 surrounding various subunits within the complex using UCSF ChimeraX and imported into
592 cryosparc2 v3.3.1 where it was lowpass filtered and dilated[3] (Extended Data Fig.2). The masks
593 were used for subsequent local refinement and resulted in improvements of the map between
594 3.02 Å – 3.72 Å (Extended Data Fig.2 and Extended Data Fig.3).
595
596 The data processing workflow for GATOR2-CASTOR1$^{apo}$- Sestrin2$^{apo}$-GATOR1 is
597 summarized in Extended Data Fig.9. In short, raw movies were imported into cryosparc2 v4.3.1
598 [2]. Patch Motion Corr. was used for motion correction and Patch CTF estimated (multi) was used
599 for CTF determination. Cryosparc blob picker with a diameter range of 180Å-230Å, 210Å-260Å
600 and 240Å-300Å were used to generate 1,344,786. Particles were extracted with a box size of
601 560x560 pixels in cryosparc2. Volumes from GATOR2-CASTOR1$^{apo}$ corresponding to full
602 complex and junk classes were imported and used for subsequent rounds of heterogenous
603 refinement. The final particle set contained 31,364 particles and a round of homogenous
604 refinement resulted in a 7.77Å map at 0.143 FSC. The final map revealed density for Sestrin2
605 bound to the GATOR2-CASTOR1$^{apo}$ cage but not GATOR1. 2D classification was used to

606 visualize the quality of the final particle set. Additionally, the particles picked using the 210Å-
607 260Å were sorted in 2D for GATOR1 particles. 2D classes corresponding to GATOR1 were
608 visualized but not bound to the GATOR2 complex.

609 Atomic Model Building and Refinement:

610 A composite map for GATOR2-CASTOR1 was generated in UCSF ChimeraX[3] by
611 aligning the local refinement maps to the overall map and combining the best portions of the
612 maps. The coordinates for GATOR2 (7UHY) and arginine bound CASTOR1 (5I2C) were rigid
613 body fitted into the composite map in UCSF ChimeraX[3]. To account for movement of the
614 GATOR2 subunits, the structure was separated into its individual subunits and each subunit was
615 rigid body fitted independently into the map. The MIOS subunit undergoes the largest
616 conformational change upon CASTOR1 binding. Due to this, the MIOS subunits of GATOR2
617 were broken down into three smaller portions encompassing the residues 43-380, 387-728 and
618 783-863. Each of these smaller portions were rigid body fit into the map. The rigid body fit
619 subunits were combined into a new model for further refinement. The model was refined using
620 iterative rounds of Phenix real-space refinement[4-6]. In between rounds of refinement, the model
621 was manually inspected for fit in the composite map. Residues outside of the map region were
622 manually removed using COOT. The CASTOR1 mutations (S111A and D304A) were manually
623 incorporated following the first iteration of refinement using COOT.

624

625 Arginine Binding Pocket Analysis:

626 Analysis of the CASTOR1 arginine binding pockets was performed using the CASTp program[7].

627

628 Structure prediction using AlphaFold3:

629 *GATOR2-CASTOR1-Sestrin2 prediction*

630 The structure model of Sestrin2, WDR24, MIOS, and 2 copies of SEH1L was generated
631 using AlphaFold3[8]. The confidence of the predicted models were assessed by pLDDT. The
632 Sestrin2-WDR24-MIOS-SEH1L-SEH1L was overlayed with each WDR24 subunit of the
633 GATOR2-CASTOR1 cryo-EM structure to generate a GATOR2-CASTOR1-Sestrin2 full
634 complex prediction.

635

636 Antibodies and chemicals

637 Reagents were obtained from the following sources: antibodies to MIOS (13557S),
638 WDR59 (53385S), FLAG (14793S), HA (3724S), S6K1 (2708S), phospho-T389-S6K1 (9234S)
639 from Cell Signaling Technology.

640

641 FLAG-M2 affinity gel (A2220) and individual powders of amino acids from Sigma
642 Aldrich; Pierce anti-HA magnetic beads (88836), Pierce protease inhibitor tablets, EDTA-free
643 (A32965) and hygromycin B (10687010) from Thermo Fisher Scientific; RPMI 1640 without
644 glucose and amino acids (R9010-01) from US Biologicals.

645

646 Mammalian Cell Culture

647 Adherent HEK293T human embryonic kidney cells were cultured in DMEM base media
648 supplemented with 10% (v/v) heat-inactivated fetal bovine serum, penicillin (100U/mL) and
649 streptomycin (100µg/mL). Cells were maintained in a humid atmosphere at 37°C and 5% $CO_2$.
650 Cells were routinely tested for mycoplasma contamination using MycoAlert Mycoplasma
651 Detection kit (Lonza, LT07-318).

652

653 Lentivirus production and infection

654 Lentiviruses were prepared by co-transfecting pLKO.1 constructs along with psPAX2 and
655 pMD2G packaging plasmids into HEK293T cells using the PEI transfection method. Viral
656 supernatant was collected 48h post-transfection and filtered using 0.45µm PES syringe filter. The
657 virus was then concentrated using Lenti-X concentrator (Takara Bio, 631232) according to
658 manufacturer's protocol, and stored at -80°C.

659 Short-hairpin oligonucleotides (shRNAs) directed against CASTOR1
660 (TRCN0000284010), MIOS (TRCN0000303645) or Luciferase (TRCN0000072243, used as a
661 non-targeting control) were cloned into the pLKO.1 lentiviral vector (The RNAi Consortium,
662 Broad Institute) according to the manufacturer's instructions.

663

664 For lentivirus infection, HEK293T cells were seeded along with concentrated virus and
665 8µg/ml polybrene (Millipore, TR-1003-G). After 24h, the media was changed to fresh media
666 supplemented with hygromycin B for selection. Experiments were performed 7 days post-
667 infection.

668

669 Transfections, amino acid starvation, cell lysis, immunoprecipitation and western blot

670 *Castor1 interaction with GATOR2*

671 Transient transfection of cDNAs into HEK293T cells was performed using the calcium
672 phosphate transfection method. Briefly, $2.10^6$ HEK293T cells were plated in 10cm dishes. 24h
673 after, cells were transfected with the appropriate pRK5-based cDNA in the following amounts:
674 2000ng METAP2, 3000ng FLAG-MIOS, 2000ng CASTOR1-FLAG, 2ng HA-S6K. The total

675 amount of plasmid DNA was normalized to 5000ng with empty pRK5 for each transfection. 6h
676 after, media containing the transfection mix was replaced with fresh media. Experiments were
677 performed 36h after.
678
679 For arginine starvation or restimulation, cells were incubated with arginine free RPMI for
680 50min and, when indicated, restimulated with 1.15mM arginine for 10min.
681 After the indicated treatments, cells were rinsed once with ice-cold PBS and lysed in lysis buffer
682 (10mM sodium-pyrophosphate, 10mM sodium-beta-glycerophosphate, 40mM HEPES, 4mM
683 EDTA, 1% Triton X-100, pH 7.4, supplemented with one EDTA-free protease inhibitor tablet per
684 50 ml). After 30min at 4°C under gentle agitation, cell lysates were cleared by centrifugation at
685 17,000 x g for 10min, 4°C. Protein concentrations were normalized across samples by BCA assay.
686 Equal amounts of proteins were incubated with 30µL of pre-washed anti-HA magnetic beads or
687 FLAG-M2 affinity gel for 2h at 4°C with end-over-end rotation. The immunoprecipitates were
688 washed three times with lysis buffer before denaturation by addition of 50µL sample buffer and
689 incubation at room temperature for 16h, 65°C for 10min or 95°C for 5min. Samples were resolved
690 by 4-20% SDS–PAGE and analyzed by immunoblotting.
691
692 *Sestrin2 interaction with GATOR2*
693 Transient transfection of cDNAs into HEK293T cells was performed using the calcium
694 phosphate transfection method. Briefly, $2.10^6$ HEK293T cells were plated in 10cm dishes. 24h
695 after, cells were transfected with the appropriate pRK5-based cDNA in the following amounts:
696 1000ng METAP2, 3000ng FLAG-MIOS, 4000ng FLAG-WDR24, 500ng HA-SESTRIN2, 2000ng
697 CASTOR1-FLAG, 2ng HA-S6K. The total amount of plasmid DNA was normalized to 5000ng

698 with empty pRK5 for each transfection. 6h after, media containing the transfection mix was
699 replaced with fresh media. Experiments were performed 36h after. For arginine or leucine
700 starvation, cells were incubated with arginine or leucine free RPMI for 50min. For restimulation,
701 arginine (1.15mM) was added to the media for 10min before lysis. Leucine (0.38mM) was added
702 to the lysates for 2h during immunoprecipitation.
703
704
705 cDNA cloning
706 Codon optimized and shRNA-resistant gene fragments (Twist Biosciences) for
707 CASTOR1-FLAG and FLAG-MIOS were cloned into the pRK5 vector. CASTOR1 and MIOS
708 mutants were generated using the site-directed mutagenesis QuikChange method. Briefly, two
709 overlapping primers containing the desired mutation in the center were designed. After PCR
710 amplification, products were DpnI digested and transformed into chemically competent *E.coli*.
711 Mutations were confirmed by Sanger sequencing (Quintara Biosciences).
712
713 qPCR confirmation shCASTOR1
714 RNA was extracted from HEK293T cells using the Aurum Total RNA Mini kit (BIORAD,
715 Cat#732-6820). Equal amounts of RNA were reverse-transcribed using the iScript Reverse
716 Transcription Supermix kit (BIORAD, Cat#177-8840). The resulting cDNA was amplified by
717 qPCR using the SsoAdvanced Universal SYBR Gren Supermix (BIORAD, Cat#172-5270). Data
718 were analyzed using the 2-ΔΔCt methods and normalized by the housekeeping genes ACTB and
719 HPRT1

The following primers were used: ACTB forward, 5'-GGACTTCGAGCAAGAGATGG-3'; ACTB reverse 5'-AGCACTGTGTTGGCGTACAG-3'; HPRT1 forward, 5'-TGACACTG GCAAAACAATGCA-3'; HPRT1 reverse 5'-GGTCCTTTTCACCAG CAAGCT-3'; CASTOR1 forward, 5'-GCCACCACCCTCATAGATGT-3'; CASTOR1 reverse 5'-AGGAGGTCACTGGGGAACTT-3'.

**Method References**


1 Mastronarde, D. N. Automated electron microscope tomography using robust prediction of specimen movements. *J Struct Biol* **152**, 36-51 (2005). https://doi.org:10.1016/j.jsb.2005.07.007

2 Punjani, A., Rubinstein, J. L., Fleet, D. J. & Brubaker, M. A. cryoSPARC: algorithms for rapid unsupervised cryo-EM structure determination. *Nat Methods* **14**, 290-296 (2017). https://doi.org:10.1038/nmeth.4169

3 Meng, E. C. *et al.* UCSF ChimeraX: Tools for structure building and analysis. *Protein Sci* **32**, e4792 (2023). https://doi.org:10.1002/pro.4792

4 Adams, P. D. *et al.* PHENIX: a comprehensive Python-based system for macromolecular structure solution. *Acta Crystallogr D Biol Crystallogr* **66**, 213-221 (2010). https://doi.org:10.1107/S0907444909052925

5 Afonine, P. V. *et al.* Real-space refinement in PHENIX for cryo-EM and crystallography. *Acta Crystallogr D Struct Biol* **74**, 531-544 (2018). https://doi.org:10.1107/S2059798318006551

6 Liebschner, D. *et al.* Macromolecular structure determination using X-rays, neutrons and electrons: recent developments in Phenix. *Acta Crystallogr D Struct Biol* **75**, 861-877 (2019). https://doi.org:10.1107/S2059798319011471

7 Tian, W., Chen, C., Lei, X., Zhao, J. & Liang, J. CASTp 3.0: computed atlas of surface topography of proteins. *Nucleic Acids Res* **46**, W363-W367 (2018). https://doi.org:10.1093/nar/gky473

8 Abramson, J. *et al.* Accurate structure prediction of biomolecular interactions with AlphaFold 3. *Nature* **630**, 493-500 (2024). https://doi.org:10.1038/s41586-024-07487-w

753 **Acknowledgements**: We thank Zhicheng Cui and Aaron Joiner for discussions, Rick Hooy for
754 workstation support, Dorotea Fracchiolla for assistance with figure preparation, and Dan Toso
755 and Ravindra Thakkar for electron microscope support.
756
757 **Funding:** This work was supported by Genentech as part of the Alliance for Therapies in
758 Neuroscience and the National Cancer Institute NIH, R01 CA285366 (J.H.H.) and
759 1R35GM149302 (R.Z.), a National Science Foundation Graduate Research Fellowship (R.M.J.).
760
761 **Author Contributions:** R.M.J. and J.H.H. conceived and designed research, R.M.J., C.M., K.T.,
762 S.W., S. Y., and X. R. carried out research, R.Z. and J.H.H. supervised research, R.M.J. and
763 J.H.H. wrote the first draft, and all authors edited the manuscript.
764
765 **Competing Interests:** J.H.H. is a co-founder and shareholder of Casma Therapeutics, recieves
766 research funding from Hoffmann-La Roche, and has consulted for Corsalex. R.Z. is a cofounder
767 and shareholder of Frontier Medicines, science advisory board member for Nine Square
768 Therapeutics and receives research funding from Genentech.
769
770 **Materials & Correspondence:** Coordinates and density are being deposited in the RCSB and
771 EMDB, respectively. Direct correspondence to rzoncu@berkeley.edu or
772 jimhurley@berkeley.edu.
773
774

775 **Extended Data**

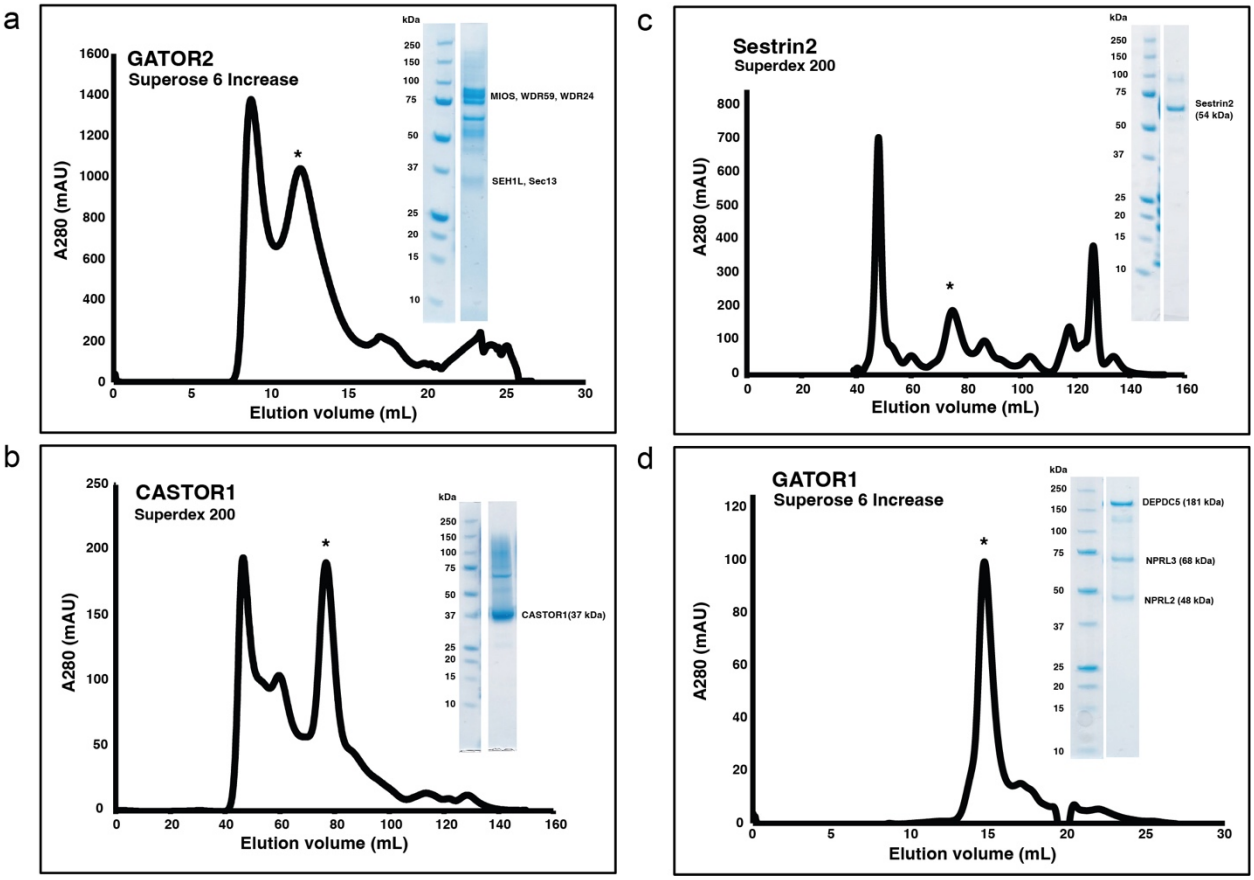


776

777

778 **Extended Fig.1: Purification for GATOR2 and CASTOR1.** (a) Chromatogram and gel for

779 GATOR2 purification. (b) Chromatogram and gel for CASTOR1 purification. (c) Chromatogram

780 and gel for Sestrin2 purification. (d) Chromatogram and gel for GATOR1 purification.

781

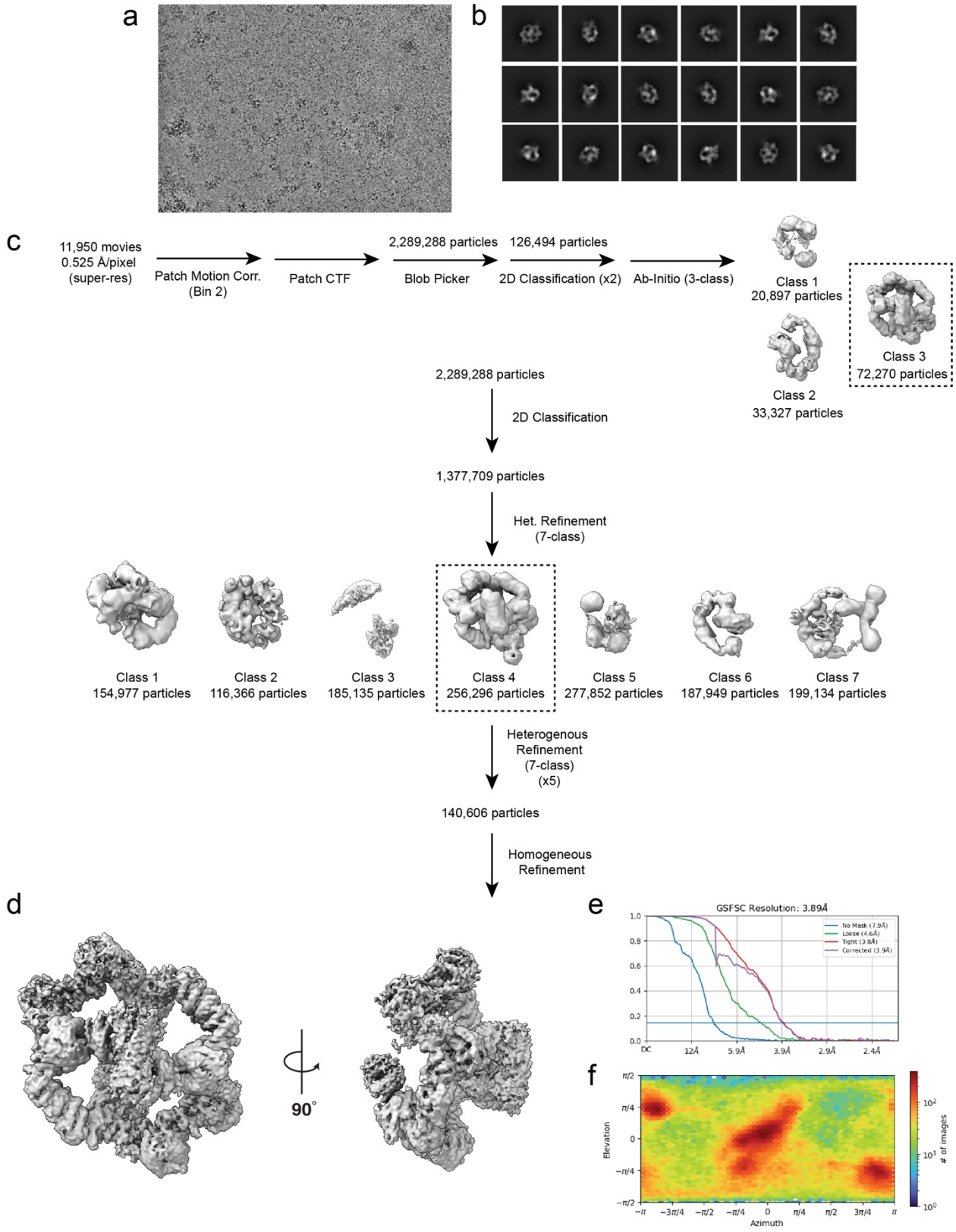
a
b
c
11,950 movies
0.525 Å/pixel
(super-res)
Patch Motion Corr.
(Bin 2)
Patch CTF
2,289,288 particles
Blob Picker
126,494 particles
2D Classification (x2)
Ab-Initio (3-class)
Class 1
20,897 particles
Class 2
33,327 particles
Class 3
72,270 particles
2,289,288 particles
2D Classification
1,377,709 particles
Het. Refinement
(7-class)
Class 1
154,977 particles
Class 2
116,366 particles
Class 3
185,135 particles
Class 4
256,296 particles
Class 5
277,852 particles
Class 6
187,949 particles
Class 7
199,134 particles
Heterogenous
Refinement
(7-class)
(x5)
140,606 particles
Homogeneous
Refinement
d
90°
e
GSFSC Resolution: 3.89Å
No Mask (7.9Å)
Loose (4.6Å)
Tight (3.8Å)
Corrected (3.9Å)
DC
12Å
5.9Å
3.9Å
2.9Å
2.4Å
f
Elevation
Azimuth
# of images

782

783 **Extended Fig.2: Data Processing Pipeline for GATOR2-CASTOR1 complex.** (a)

784 Representative micrograph (b) Representative 2D classes (c) Data processing workflow (d)

785 Overall map for GATOR2-CASTOR1 (e) FSC graph (f) Orientation plot.

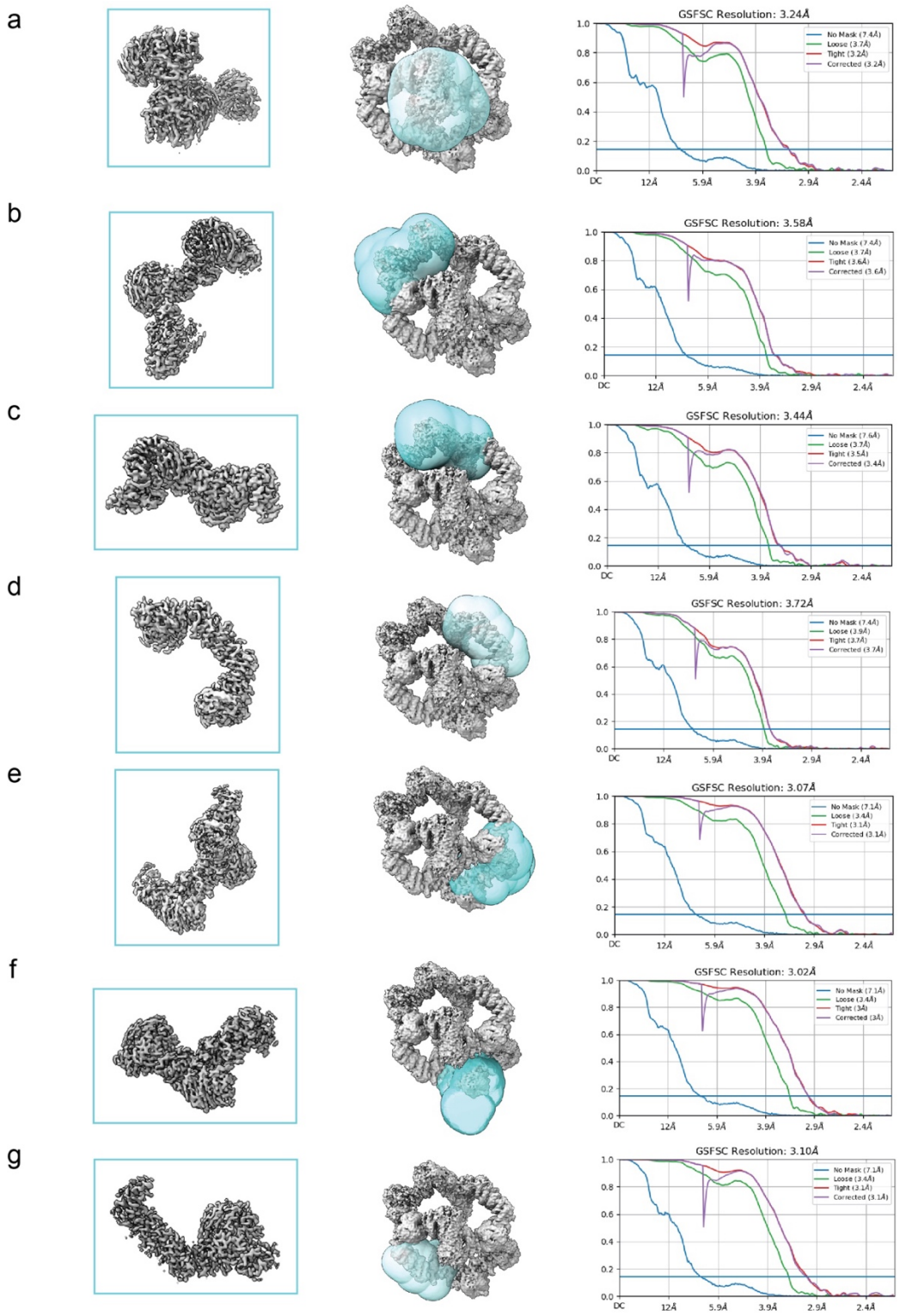


**Extended Fig. 3: Local Refinement for GATOR2-CASTOR1.** (a-g) Local refinement for different sections of complex. Including mask (shown in cyan), FSC graph and resulting map.

789

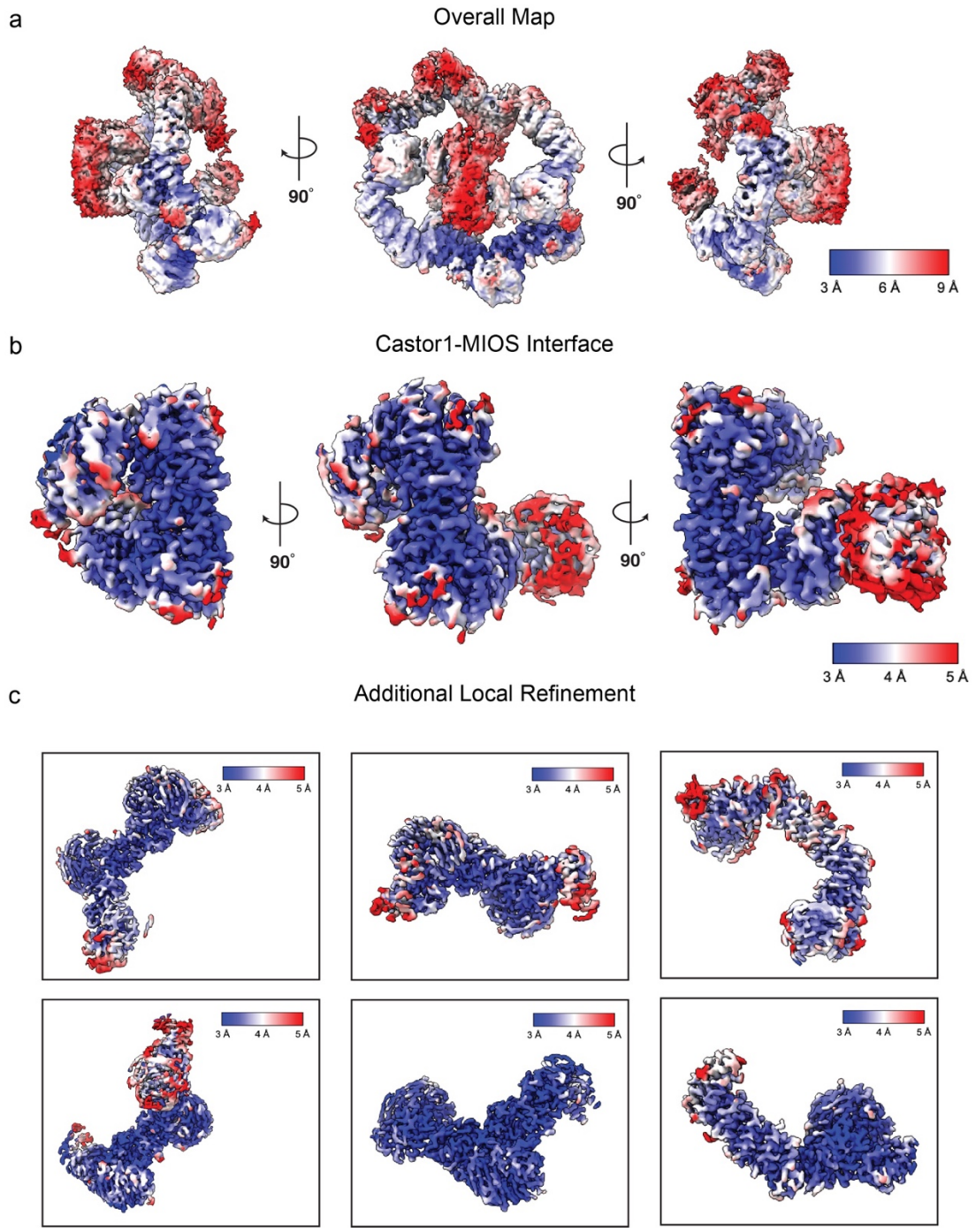


790

791

792 **Extended Fig. 4: Local resolution estimation.** (a) Full complex map (b) CASTOR1-MIOS

793 interface and (c) additional local refinement maps for the complex.

794

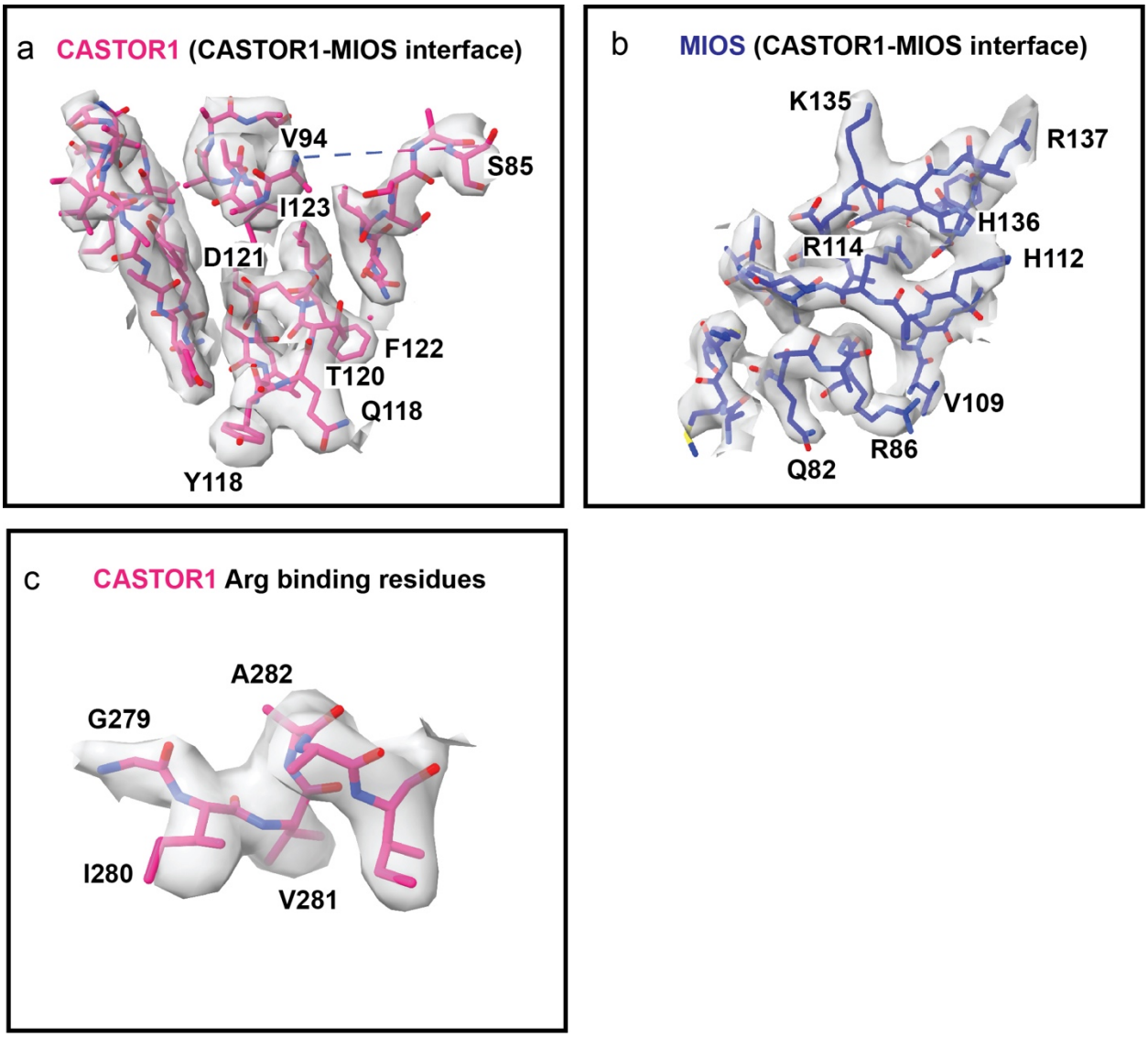


**Extended Fig. 5: Map to model fit.** (a) CASTOR1 at CASTOR1-MIOS interface, (b) MIOS at CASTOR1-MIOS interface (c) CASTOR1 residues near arginine binding pocket.

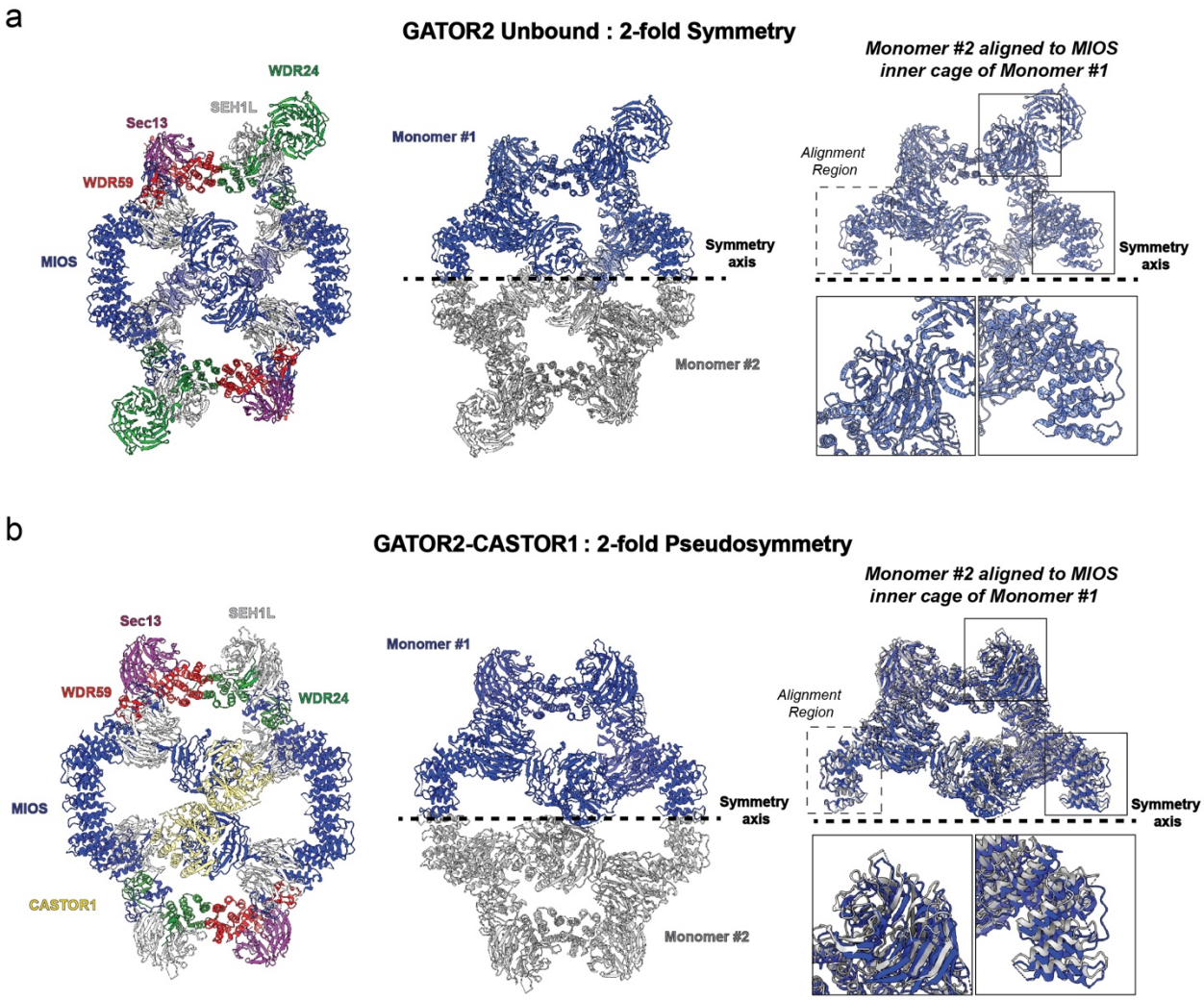


**Extended Fig. 6: GATOR2 Cage Symmetry.** Comparison of cage symmetry for (a) GATOR2 unbound and (b) GATOR2-CASTOR1 complex. For each complex the individual monomers are reflected over the symmetry axis. Regions distal to the alignments region are enlarged for visualization.

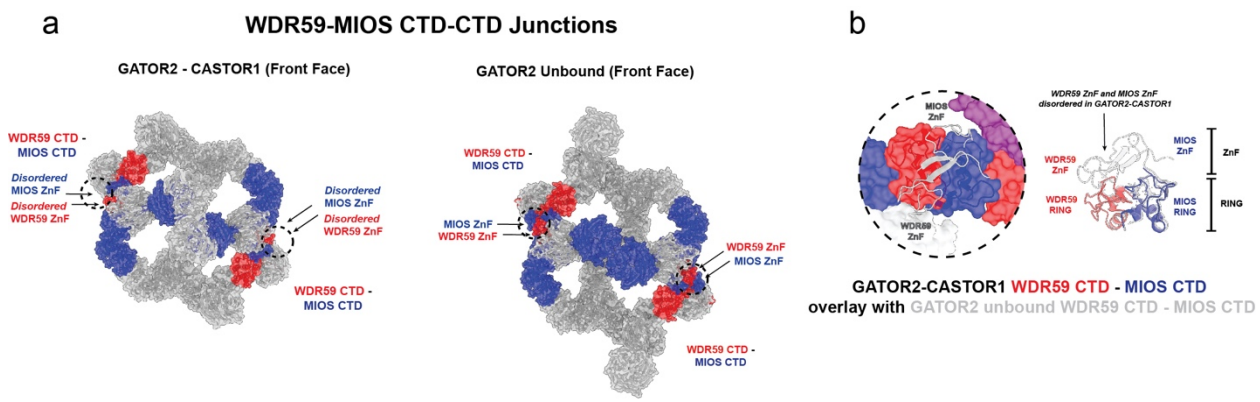


**Extended Fig. 7: GATOR2 WDR59-MIOS CTD-CTD Junctions.** (a) Comparison of the WDR59-MIOS junctions (black dash circle) on GATOR2-CASTOR1 complex and GATOR2 unbound. (b) Close up view of the changes to the WDR59-MIOS CTD junctions. GATOR2 unbound (grey) overlayed with the GATOR2-CASTOR1 (blue and red).

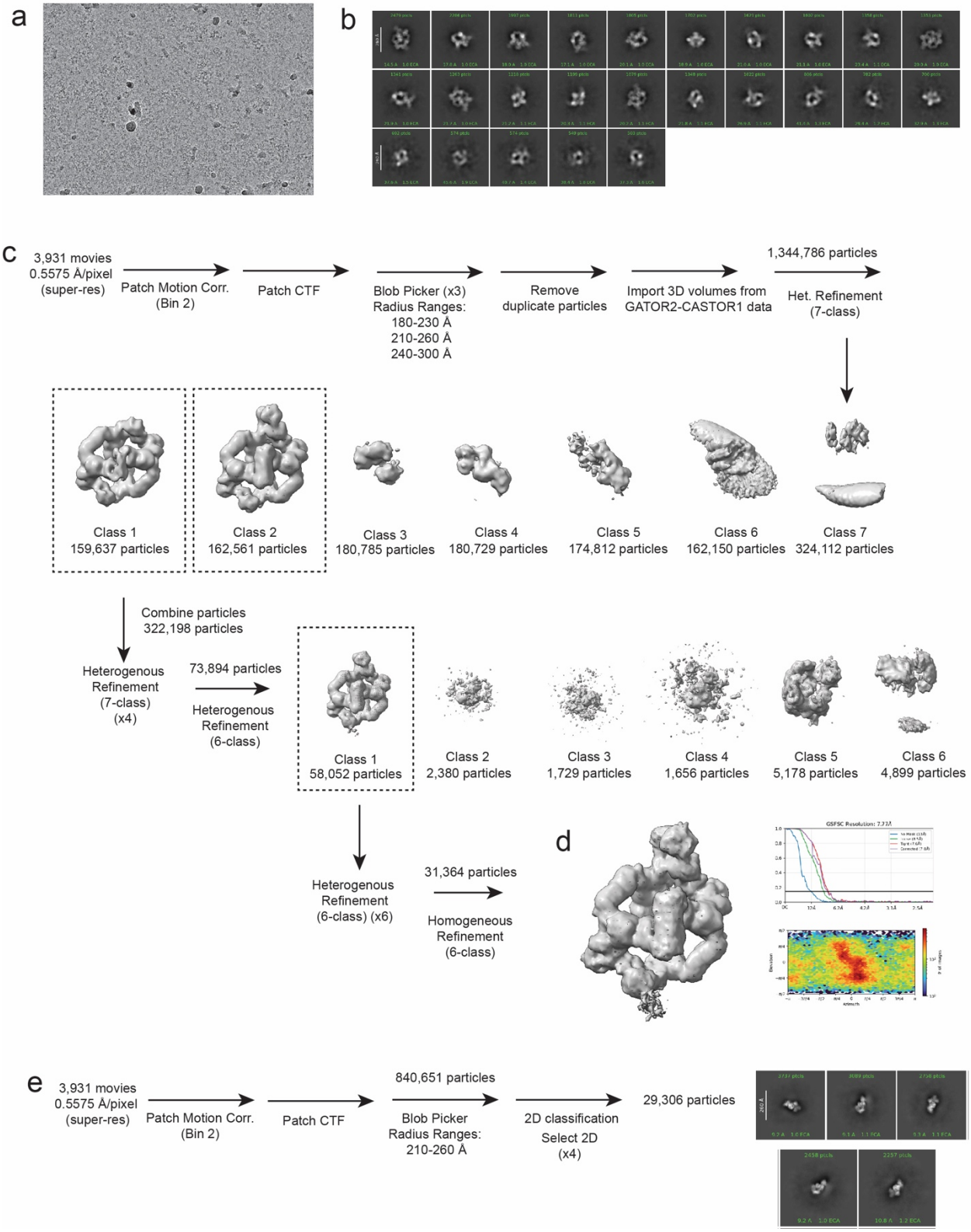
a
b
c
3,931 movies
0.5575 Å/pixel
(super-res)
Patch Motion Corr.
(Bin 2)
Patch CTF
Blob Picker (x3)
Radius Ranges:
180-230 Å
210-260 Å
240-300 Å
Remove
duplicate particles
Import 3D volumes from
GATOR2-CASTOR1 data
1,344,786 particles
Het. Refinement
(7-class)
Class 1
159,637 particles
Class 2
162,561 particles
Class 3
180,785 particles
Class 4
180,729 particles
Class 5
174,812 particles
Class 6
162,150 particles
Class 7
324,112 particles
Combine particles
322,198 particles
Heterogenous
Refinement
(7-class)
(x4)
73,894 particles
Heterogenous
Refinement
(6-class)
Class 1
58,052 particles
Class 2
2,380 particles
Class 3
1,729 particles
Class 4
1,656 particles
Class 5
5,178 particles
Class 6
4,899 particles
Heterogenous
Refinement
(6-class) (x6)
31,364 particles
Homogeneous
Refinement
(6-class)
d
e
3,931 movies
0.5575 Å/pixel
(super-res)
Patch Motion Corr.
(Bin 2)
Patch CTF
840,651 particles
Blob Picker
Radius Ranges:
210-260 Å
2D classification
Select 2D
(x4)
29,306 particles

820

821 **Extended Fig. 8. Data Processing Pipeline for GATOR2-CASTOR1-Sestrin2.** (a)

822 Representative micrograph (b) Representative 2D classes (c) Data processing workflow (d)

823 Overall map for GATOR2-CASTOR1, FSC graph and orientation plot. (e) Data processing for

824 GATOR1 and representative 2D classes of isolated GATOR1 complex particles.

825
826

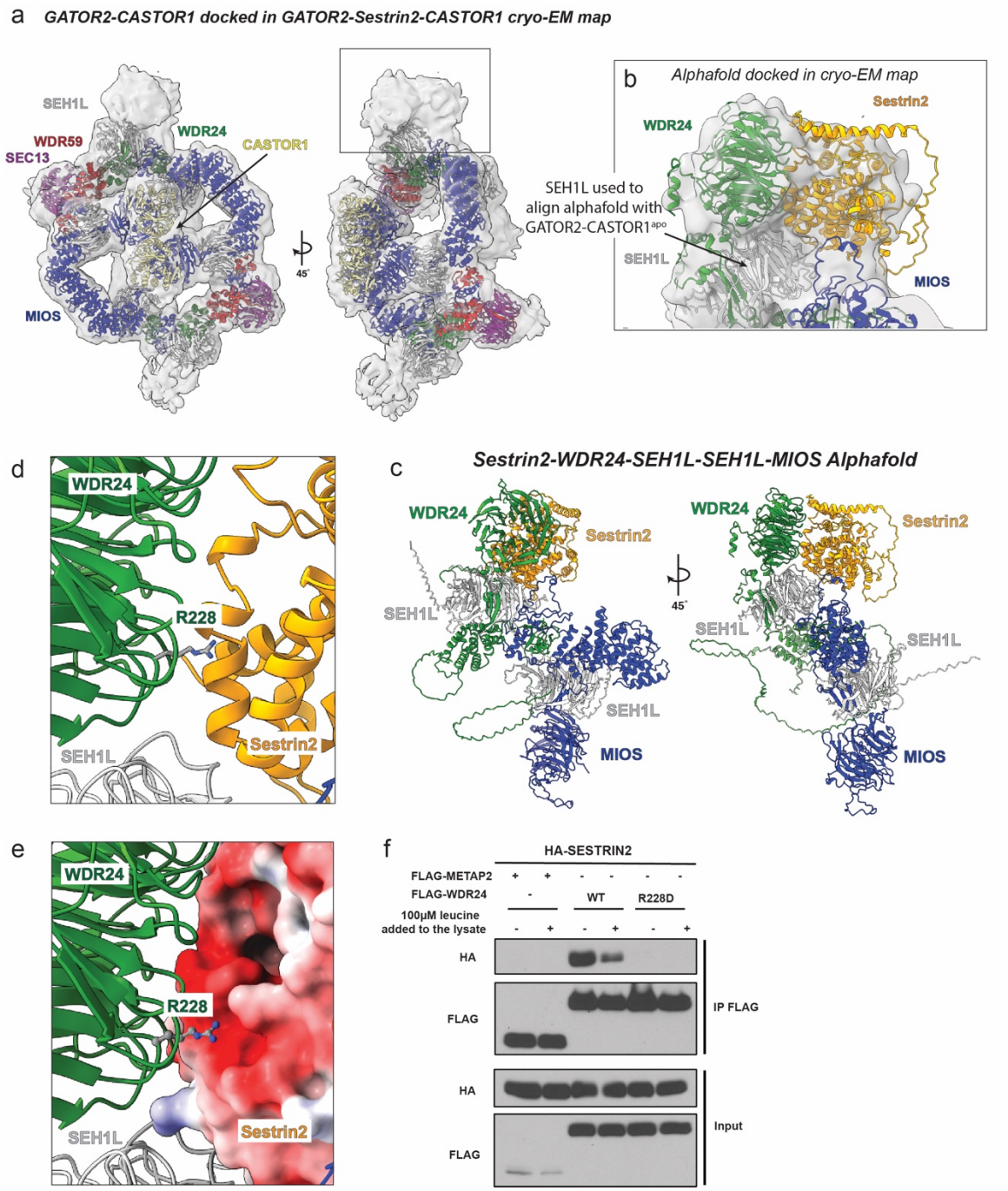


827

828

829 **Extended Fig. 9: GATOR2-CASTOR1- Sestrin2 interaction.** (a) GATOR2-CASTOR1

830 structure docked into cryo-EM map of GATOR2-CASTOR1-Sestrin2. (b) Close up of GATOR2-

831 CASTOR1-Sestrin2 cryo-EM density fitted with Sestrin2-WDR24-SEH1L-SEH1L-MIOS

832 AlphaFold model (c) Full Sestrin2-WDR24-SEH1L-SEH1L-MIOS AlphaFold model (ipTM =
833 0.69). Close up of interface between WDR24 (green) and Sestrin2 (orange) in AlphaFold model
834 in (d) ribbon view and (e) surface view colored by electrostatic potential. pLDDT for Arg 228 is
835 0.89. (f) HEK-293T cells transiently expressing HA-tagged SESTRIN2 along with the indicated
836 FLAG-tagged WDR24 constructs or FLAG-tagged METAP2 as a control were starved of leucine
837 for 50 minutes. Where indicated, leucine was added to the lysates during immunoprecipitation.
838 FLAG-immunoprecipitates were generated and analyzed by immunoblotting for the indicated
839 proteins.
840
841
842
843
844
845
846
847

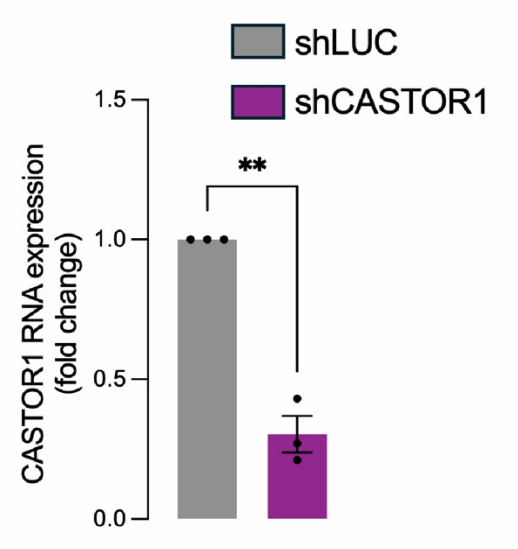


848

849 **Extended Fig. 10: qPCR confirmation shCASTOR1.** qPCR against CASTOR1 performed in

850 HEK293T transduced with a shRNA targeting Luciferase (shLUC) or a shRNA targeting

851 CASTOR1. Data were normalized using ACTB and HPRT1 as housekeeping genes.

852

853 **Extended Data Movie 1: Structural rearrangement of GATOR2 upon interaction with**

854 **CASTOR1.** Visualization of GATOR2 prior to interaction with CASTOR1. CASTOR1 appears

855 and GATOR2 reorients to engage CASTOR1 through MIOS subunits.

856
857

858

859

860 **Extended Data Table 1: Cryo-EM data acquisition and image processing.**
861

| | GATOR2-CASTOR1 complex | GATOR2-CASTOR1-Sestrin2 Complex |
|---|---|---|
| **Data acquisition** | | |
| Microscope | Titan Krios | Talos Arctica |
| Voltage (kV) | 300 | 200 |
| Camera | GATAN K3 | GATAN K3 |
| Magnification | 165,000 | 36,000 |
| Pixel size (Å) | 0.525 (super-resolution) | 0.558 (super-resolution) |
| Cumulative exposure ($e^-/Å^2$) | 50 | 50 |
| Energy filter slit width (eV) | 20 eV | |
| Defocus range (μm) | -1.0 to -2.0 | -1.0 to -2.0 |
| Automation software | SerialEM | SerialEM |
| Exposure navigation | Image Shift | Image Shift |
| Number of movies | 11,950 | 3,931 |
| **Image processing** | | |
| Initial picked particles (no.) | 2,289,288 | 1,344,786 |
| Final refined particles (no.) | 140,606 | 31.364 |
| Map resolution (Å) | Overall: 3.02-3.72, Interface: 3.24 | Overall: 7.77 |
| FSC threshold | 0.143 | |

862
863

864

865 **Extended Data Table 2: GATOR2-CASTOR1 coordinate model refinement and assembly**
866

| | |
|---|---|
| **PDB access code** | |
| **EMDB** | |
| | |
| **Refinement** | |
| Software | Phenix 1.19 |
| Refinement target (Å) | 3.24 (interface) 3.89 (overall) |
| Non-hydrogen atoms | 43,315 |
| Residues | 6,081 |
| GATOR2 reference PDB | 7UHY |
| CASTOR1 reference PDB | 5I2C |
| | |
| **Map-model statistics** | |
| R.M.S deviations | |
| Bond lengths (Å) | 0.002 |
| Bonds angles (Å) | 0.453 |
| | |
| **Validation** | |
| Molprobitity | 1.56 |
| Clash score | 8 |
| Rotamer ouliers (%) | 0.03 |
| Cβ outliers (%) | 0.00 |
| CaBLAM outliers (%) | 1.23 |
| Ramachandran | |
| Favored (%) | 0.03 |
| Allowed (%) | 2.59 |
| Outlier (%) | 97.37 |
| | |
| **Final model composition** | |
| Number of chains | 18 |
| Number of Residues | 6,081 |
| B-factors | |
| Protein (min/max/average) | 23.7/140.37/74.06 |

867
868
869
870
871
872
873
874
875
876
877

878
879

## Supplementary Files

This is a list of supplementary files associated with this preprint. Click to download.

- EDMovie1.mp4